Title
Film and membrane-model thermodynamics of free thin liquid films

Author
Radke, CJ

Publication Date
2015-07-01

DOI
10.1016/j.jcis.2014.12.079

Peer reviewed

Journal of Colloid and Interface Science 449 (2015) 462–479

Contents lists available at ScienceDirect

Journal of Colloid and Interface Science

www.elsevier.com/locate/jcis

Film and membrane-model thermodynamics of free thin liquid films

C.J. Radke *

Department of Chemical and Biomolecular Engineering, University of California, Berkeley, CA 94720-1462, United States

GRAPHICAL ABSTRACT

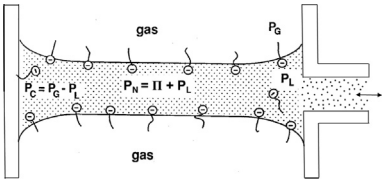

ARTICLE INFO

Article history:
Received 17 November 2014
Accepted 23 December 2014
Available online 31 December 2014

Keywords:
Thin films
Conjoining/disjoining pressure
Film model
Membrane model
Thin-film Gibbs adsorption equation
Modified Young–Laplace relation
Film contact angle
Frumkin–Deryagin equation
Square-gradient theory
Molecular simulation

ABSTRACT

In spite of over 7 decades of effort, the thermodynamics of thin free liquid films (as in emulsions and foams) lacks clarity. Following a brief review of the meaning and measurement of thin-film forces (i.e., conjoining/disjoining pressures), we offer a consistent analysis of thin-film thermodynamics. By carefully defining film reversible work, two distinct thermodynamic formalisms emerge: a film model with two zero-volume membranes each of film tension γ^f and a membrane model with a single zero-volume membrane of membrane tension $2\gamma^m$. In both models, detailed thermodynamic analysis gives rise to thin-film Gibbs adsorption equations that allow calculation of film and membrane tensions from measurements of disjoining-pressure isotherms. A modified Young–Laplace equation arises in the film model to calculate film-thickness profiles from the film center to the surrounding bulk meniscus. No corresponding relation exists in the membrane model.

Illustrative calculations of disjoining-pressure isotherms for water are presented using square-gradient theory. We report considerable deviations from Hamaker theory for films less than about 3 nm in thickness. Such thin films are considerably more attractive than in classical Hamaker theory. Available molecular simulations reinforce this finding.

1. Introduction

Emulsions and foams are important dispersions with large application in industrial technologies. When two suspended bubbles or drops come into close contact, the continuous liquid separating the dispersed phases thins, eventually flattening the bubbles or drops in the contact region. If the intervening gap separation is small enough, thin films emerge. Whenever the bounding interfaces are both fluid, the film is referred to as a free thin liquid film.

All free thin liquid films are thermodynamically unstable because coalescence reduces the overall system surface area and, accordingly, diminishes the system free energy. However, net repulsive interaction forces arising in free thin liquid films can impart considerable metastability. Indeed, some foams and emulsions are persistent enough to warrant considerable efforts to destroy them.

The governing interaction forces in free thin films have held the attention of colloid scientists for many decades. Although both attractive (conjoining) and repulsive (disjoining), Deryagin and coworkers defined "disjoining pressure" to quantify thin-film interaction forces [1–5]. Much of the early work is in Russian, but a helpful summary of the initial work became available in 1987 [6]. Scheludko and coworkers in the 1960s were the first to

* Address: Department of Chemical and Biomolecular Engineering, University of California, Berkeley, 101E Gilman Hall, Berkeley, CA 94720-1462, United States. Fax: +1 510 642 4778.
E-mail address: radke@berkeley.edu

http://dx.doi.org/10.1016/j.jcis.2014.12.079
0021-9797/

measure film thickness by thin-film micro-interferometry thereby launching continuing studies on disjoining-pressure isotherms in what is now called a "Scheludko cell" [7–9]. In the 1980s, the school of Wasan pioneered in bringing concepts of disjoining/conjoining forces in free thin films to the forefront of colloid research specifically in the areas of structural forces and film-drainage kinetics [10–37].

In stable (i.e., metastable) thin films, disjoining pressure is a reversible function of film thickness so that thermodynamic principles apply. After a brief summary in Section 2 of thin-film definitions and concepts, we focus on the thermodynamics of free thin liquid films. A large effort is available on this topic [6,38–58]. Fascinatingly, much of it is contradictory due to the lack of consistent definition of film properties in terms of density distributions. In Section 3, we present two self-consistent Gibbs thermodynamic frameworks to describe thin-film equilibria: a film model and a membrane model. Careful definition of the reversible work to expand/contract flat thin films leads to two different definitions of surface tension in thin films. In the film model, two interfaces are present bounding a bulk liquid film and surrounded by vapor. In the membrane model, no liquid film is present, only a zero-thickness membrane surrounded by vapor. A modified Young–Laplace equation emerges within the film model to predict film-thickness profiles adjacent to a bulk meniscus. The modified Young–Laplace equation reduces to the classic augmented Young Laplace equation [4–6] under well-defined approximations. No film-thickness profiles exist in the membrane model. Film contact angle is derived for both film and membrane models consonant with the classic Deryagin–Frumkin equation [4,5,59] but with different meanings of film thickness. Section 4 illustrates the thin-film thermodynamic formulations using square-gradient theory (SGT) for a single-component flat film. Brief review is then made of available molecular simulations of free thin liquid films, followed by Conclusions.

2. Background

2.1. Definition

Fig. 1 presents molecular-dynamics simulations of one half of the mass-density profile, $\rho_w(z)$, across a thin water film surrounded by water vapor at 479 K [60]. Five films of differing thickness are shown. Thinner films merge into the vapor phase at smaller z values. The thickest film, Film 1, attains the bulk density of water at the film center and exhibits negligible thin-film forces. Remaining thinner films do not reach a centerline bulk density. The thinner is the film, the lower is the center mass density relative to that in the bulk. The definition of a thin film is that nowhere in the film is a bulk thermodynamic density reached. This definition holds not only for mass density, but, for example, also for energy density (i.e., $\tilde{u}(z) = U/V$) or entropy density (i.e., $\tilde{s}(z) = S/V$). Film 1 in Fig. 1 is a bulk liquid film, whereas Films 2–5 are thin films. Surface tension in Film 1 corresponds to the bulk value, whereas Films 2–5 do not exhibit a bulk surface tension. According to Fig. 1, completely inhomogeneous (i.e., thin) films of water appear at about 2-nm thickness or at about 8 layers of closed-packed water molecules. Because no bulk liquid property exists within a thin film, definition of interface excess properties requires thought. We must identify excess interface thermodynamic properties relative to properties other than those actually in the inhomogeneous film.

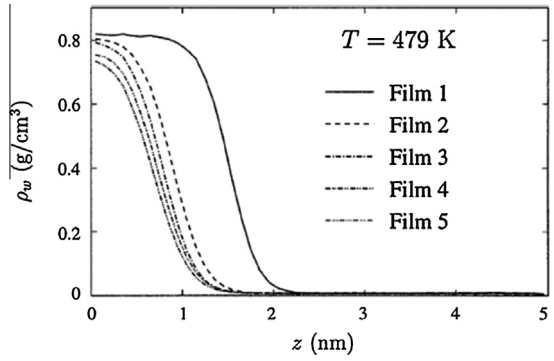

Fig. 1. Mass-density profiles of water in free liquid thin films from molecular simulation. Reprinted with permission from Bhatt et al. [60].

Free thin films are classified by the fluids surrounding the liquid from which the film is formed. Foams correspond to a liquid film surrounded by gas. Emulsions correspond to liquid films surrounded by a second immiscible liquid, such as oil-in-water or water-in-oil dispersions. A liquid film surrounded by gas on one side and an immiscible liquid on the other is coined a pseudo-emulsion film. Gas films surrounded by liquids do not bare a moniker, apparently because their short life times do not permit extensive study.

Thin fluid films that abut against at least one solid phase are also defined by exhibiting no bulk property within the film. If the second interface of the film is adjacent to a fluid, the films are designated as adsorbed or wetting depending on film thickness. If, however, the second interface of the film is also a solid, the film is designated as confined. The distinguishing feature of solids is the lack of well-defined equilibrium stresses. Accordingly, the solid/fluid interface is usually treated as solid atoms exerting an external force on the fluid molecules. No external force field is present in free thin films. Although we focus on free liquid thin films, many of the concepts apply to adsorbed/wetting and confined thin films.

2.2. Disjoining pressure

Fig. 2 illustrates the definition of disjoining pressure originally put forth by Deryagin et al. [1–6]. A flat foam film (highlighted by dots) terminates at a capillary wall through a liquid meniscus known as a Plateau border [61–63]. In Fig. 2, the film is stabilized by adsorbed anionic surfactant. A small port in the capillary wall permits injection/withdrawal of liquid at pressure P_L into or out of the meniscus thereby thickening/thinning the film. The gas phase is at pressure P_G. In the absence of external forces, conservation of momentum demands that divergence of the stress tensor in the film is zero. Consequently, the normal stress in the flat film, P_N, is constant across film thickness [51,62–67]. According to the law of Young–Laplace, the product of bulk-meniscus curvature and surface tension is balanced by a pressure difference between the gas

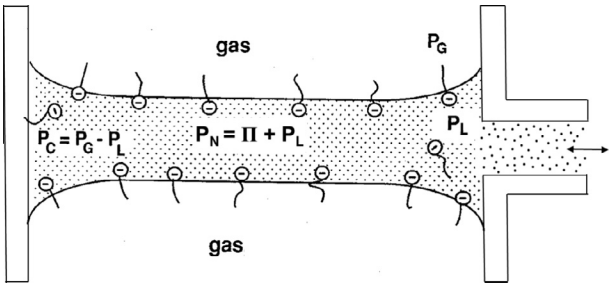

Fig. 2. Schematic of a Sheludko cell. A surfactant-stabilized foam film exhibiting disjoining pressure Π is formed inside a capillary. Disjoining pressure balances the imposed capillary pressure on the film. Liquid is injected/withdrawn through a side port to probe various thickness films. Drawing is not to scale.

and liquid phases in the Plateau border and is designated as the capillary pressure [62–67]

$$P_C \equiv P_G - P_L = 2\gamma C_m \quad \text{bulk meniscus} \tag{1}$$

where γ is surface tension and C_m is the meniscus mean curvature. Because the meniscus is convex to the gas phase, liquid pressure is lower than that in the gas phase. In the flat film, however, curvature is zero. Here, the Young–Laplace law enforces equality of normal stress across the two interfaces of the film or $P_G = P_N$. Thus, the liquid pressure in the meniscus is lower than the normal pressure in the flat film to which it is connected. Mechanical equilibrium is not satisfied; the film drains.

To permit (metastable) equilibrium, Deryagin postulated the existence of disjoining forces per unit area of film, Π, the disjoining pressure [1–6]. Thus, as illustrated in Fig. 2, the normal pressure in the liquid film is larger than that in the meniscus liquid by the magnitude of the disjoining pressure: $P_G = P_N = P_L + \Pi$. Because the gas pressure is everywhere constant, mechanical equilibrium between the flat film and the meniscus is, accordingly, established by equality of capillary and disjoining pressures

$$P_C = P_G - P_L = \Pi \quad \text{flat film} \tag{2}$$

Eq. (2) defines disjoining pressure. The capillary-suction pressure in the bulk meniscus is balanced by disjoining pressure in the flat film. At equilibrium, chemical potentials of all components in the system are uniform and equal in the film, the gas phase, and the liquid meniscus [51]. However, bulk liquid in the meniscus is at a lower pressure than that in the gas phase. For a pure liquid, this means that the meniscus liquid lies along a pressure/volume isotherm at a pressure below the binodal value while the high-pressure gas phase lies above the binodal value. Neither phase exhibits the binodal saturation vapor pressure.

As the flat film transitions continuously into the bulk-liquid meniscus in Fig. 2, curvatures of the two film interfaces increase as does film thickness. P_C for (meta)stable thin films is a positive constant. To maintain a constant capillary pressure as curvature rises, disjoining pressure falls laterally along the film interfaces toward the bulk meniscus. This idea undergirds the augmented Young–Laplace equation and is discussed further in Section 3.7. The conclusion is that in regions of film thickness where free thin films are stable, disjoining pressure is a positive, decreasing function of film thickness, h (i.e., $\Pi > 0$ and $d\Pi/dh < 0$).

Eq. (2) provides the foundation to measure disjoining-pressure isotherms. Bulk liquid in the Scheludko cell [7–9] of Fig. 2 is injected/withdrawn at measured gas and liquid pressures setting the capillary pressure and, hence, the equilibrium disjoining pressure: $P_C = \Pi$. Once film thickness stabilizes, it is usually measured by micro-interferometry [7–9]. Since film thickness is optically determined, it may not be identical to that defined thermodynamically. Disjoining-pressure isotherms, $\Pi(h)$, are probed only along positive stable branches. Typically in a Scheludko cell, the gas phase is exposed to atmosphere while the liquid solution is at sub-atmospheric pressure.

The radius of the side port in a Scheludko cell limits the maximum capillary pressure (i.e., maximum disjoining pressure) that can be applied. To overcome this deficiency, Mysels and Jones [68] replaced the capillary in Fig. 2 by an annular liquid-wetting porous plate. The thin film is formed in the tapered bore of the porous plate. Fig. 3 illustrates the cell. It proves convenient to encase the annular porous disk in a sealed chamber where gas pressure is adjusted to set the capillary pressure. Film thickness is measured by the micro-interferometry technique of Scheludko [7–9]. Fig. 4 shows the necessary ancillary equipment of a measuring cell. Details may be found elsewhere [9,69–71].

Fig. 5 reports example disjoining-pressure isotherms here for an aqueous solution of 10^{-3}-M sodium dodecyl sulfate (SDS) below

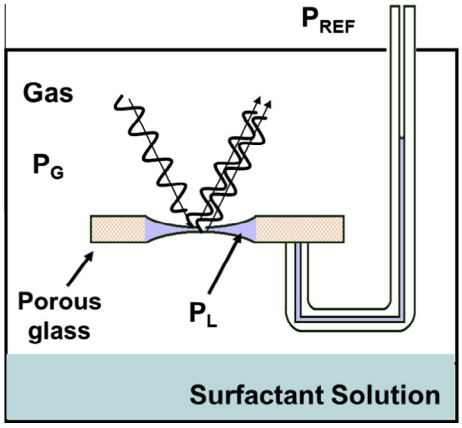

Fig. 3. Schematic of a Mysels cell to measure disjoining-pressure isotherms [68,69]. A center-bored porous plate is encased in a sealed chamber. Gas pressure is increased relative to atmospheric setting the capillary pressure. Film thickness is obtained from micro-interferometry [7–9]. Drawing is not to scale.

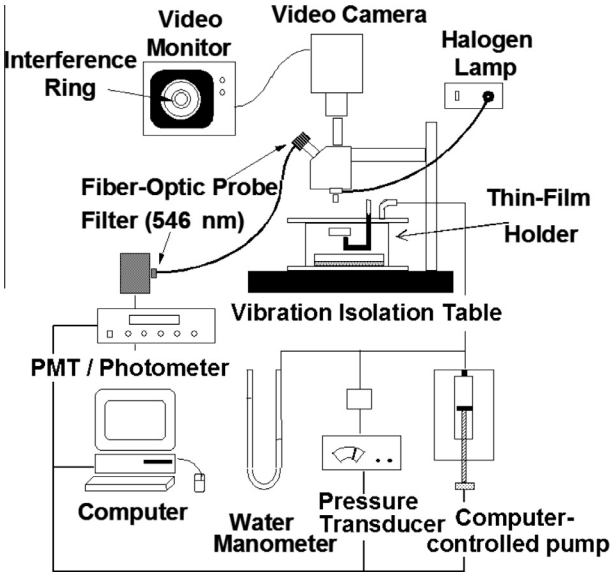

Fig. 4. Schematic of apparatus to measure disjoining-pressure isotherms with a porous-plate cell. A halogen lamp illuminates the film. Reflected light is transmitted through a fiber-optic probe to a photometer allowing thickness measurement. Gas pressure is carefully set by a computer-controlled pump and measured by a pressure transducer. A video camera allows film visualization. Reprinted with permission from Bergeron and Radke [69].

the critical micelle concentration [71]. Typical values for disjoining pressure are of order kPa. With no added salt and with 10^{-2}-M added NaCl, films are weak and rupture near 1 kPa close to 20 nm in thickness. Rupture is statistical with the symbol R locating the lowest-observed rupture pressure. Films are reversible below the rupture pressure. As salt concentration increases to 0.18 M, films are stronger and thinner with a steeper isotherm. Again reversible traverses along the isotherm can be made. Above about 0.25-M NaCl, instead of rupture, a second, very steep isotherm branch appears near 4.5 nm in thickness. This inner branch does not rupture up to the maximum allowed capillary pressure of the particular porous plate. Both branches of the 0.25-M NaCl isotherm are again reversible. Nonetheless, there is a difference in behavior between thinning and thickening the films. Upon thinning, the outer film transitions directly to the inner branch. Upon thickening of the inner branch, however, the outer branch does not appear. Rather, the film thickens to a biconcave meniscus.

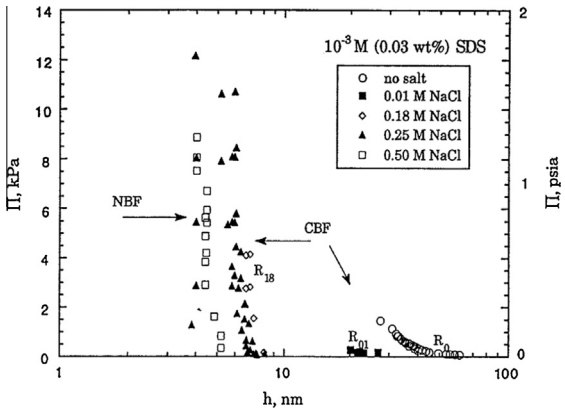

Fig. 5. Ambient-temperature disjoining-pressure isotherms of aqueous sodium dodecyl sulfate (SDS) for increasing NaCl concentrations. The symbol R labels the lowest observed rupture pressure along the particular isotherm branch. Symbols NBF and CBF denote Newton black films and common black films, respectively. Reprinted from Aronson et al. [71] with permission.

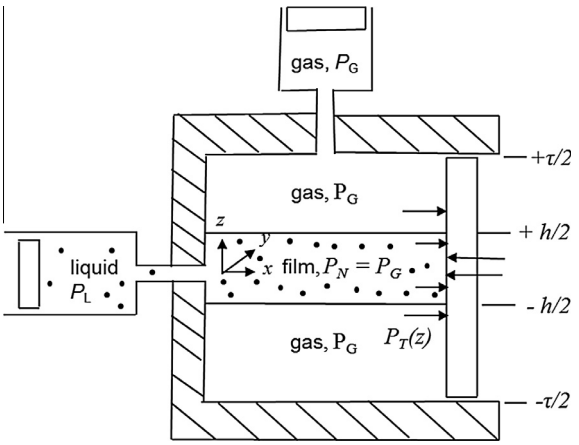

Fig. 6. A rectangular box of width w out of the paper and containing a free thin liquid film (shown dotted). The upper gas reservoir is connected to the gas below the film (not shown). $P_G > P_L$ due to terminating menisci (not shown). The right piston is infinitesimally translated to the right while the gas-reservoir and liquid-reservoir pistons are infinitesimally depressed to maintain constant film thickness. Drawing is not to scale.

Details of the thinning transitions between branches are well documented [12,16,19,21,22,72]. Thin inner-branch films are designated as Newton black films (NBF), whereas outer thicker films are designated as common black films (CBF). These designations conform to the early Russian observations of α and β branches of wetting films [6]. CBFs in Fig. 5 are amenable to DLVO theory [62,63,73]. The molecular origin of disjoining forces in Newton black films, however, is not completely clear [74]. Water and ion structuring are paramount in these thin films [75–77].

The main feature of measured disjoining-pressure isotherms pertinent here is that they are reversible functions of film thickness. Thermodynamic analysis is applicable. Measurement of isotherms for identical chemical systems is reproducible among various laboratories using differing apparatus [69]. Somewhat differing-size films in Mysels porous-plate cells or Scheludko capillary cells yield identical isotherms within experimental error. This means that disjoining-pressure isotherms, such as those in Fig. 5, are a material property characteristic of the chemical system and not the apparatus. This finding demands that film thickness is an intensive thermodynamic variable.

3. Thermodynamics

Thermodynamic analysis of free thin liquid films rests on two disparate views. In the first analysis, the film is viewed as a homogeneous liquid slab of finite thickness h with two zero-volume interfaces and surrounded by a homogeneous vapor phase. This is, perhaps, the most common viewpoint. In the second treatment, the film is conceived as a single zero-volume membrane encompassed by homogeneous vapor. We designate the first alternative as the "film" model and the second as the "membrane" model. Each has its own definition of surface tension. In either case, the key to the thermodynamic analysis is the reversible mechanical work [78] to enlarge/diminish film thickness and to expand/contract film area.

3.1. Film-model tension

In the film model, work expressions to expand/contract film area and to enlarge/diminish film thickness are different. The first corresponds to work against film surface tension, whereas the second corresponds to work against disjoining pressure.

Fig. 6 illustrates a simple thermodynamic system to establish the reversible work for expanding (contracting) a liquid film. A gravity-free thin liquid film of thickness h and container xy-cross-sectional area A is enclosed in a rectangular parallel-piped, translationally invariant in the y direction, and in direct communication with a bulk liquid reservoir. The entire surrounding continuous gas phase is similarly connected to a separate gas reservoir. The right wall of the rectangular container is an inert frictionless piston allowing film expansion/contraction. Height of the rectangular container, τ, is much larger than film thickness; precise definition of film thickness remains to be specified. The menisci connecting the film with the liquid reservoir and with the container wall are not shown for convenience.

As opposed to confined thin films, free liquid films are not subject to an external field. Accordingly, the divergence of the stress tensor is zero [51,63–67]. The film is assumed transversely isotropic meaning that all properties are independent of coordinates x and y, but they do vary normal to the film (in the z direction). These two statements demand that the normal pressure in the film, P_N, is constant independent of the z coordinate and, therefore, equals the surrounding homogeneous gas pressure, P_G. Conversely, the tangential stress, $P_T(z)$, varies normal to the film until it attains the gas pressure outside the film. Arrows in Fig. 6 indicate schematically the film tangential stress acting on the piston. Temperature, as well as chemical potentials of all components, are equal throughout the system and accompanying reservoirs [51]. However, the pressure in the bulk liquid reservoir, P_L, is not identical to that in the gas phase surrounding the film due to curvature of the meniscus. As mentioned above, equality of component chemical potentials for phases with unequal pressure means that the bulk-gas and meniscus-liquid phases do not lie on the binodal phase envelope but rather along the pressure–volume isotherm in the metastable regions between the binodal and spinodal envelopes. From Eq. (2), the difference between the bulk gas and liquid pressures (i.e., the capillary pressure) defines the disjoining pressure. Composition of the reservoir liquid phase is not that of the film which is inhomogeneous (in the z direction). By definition, there is no bulk region in thin films (see Fig. 1).

Consider an infinitesimal withdrawal of the film-container right piston in Fig. 6 while simultaneously inserting the gas-reservoir and liquid-reservoir pistons such that film area increases at constant film thickness. No fluid volumes change magnitude. The net result of this process is film-area expansion with no change in total gas and liquid volumes. Film center of mass simply shifts to the right [78].

Differential reversible work for this process is given by

$$dW^{f}_{rev1} = -2dA\int_0^{\tau/2} P_T(z)dz - P_G dV_{GR} - P_L dV_{LR} \quad \text{constant } T \tag{3}$$

where again A is the container xy-cross-sectional area or equivalently, the single-interface area of the film. Subscripts GR and LR denote the gas and liquid reservoirs, respectively. During piston withdrawal (insertion) liquid-reservoir and gas-reservoir volumes change according to

$$dV_{GR} = -(\tau - h)dA \quad \text{and} \quad dV_{LR} = -hdA \tag{4}$$

Substitution of this result into Eq. (3) gives

$$dW^{f}_{rev1} = 2dA\left\{\int_0^{h/2}[P_L - P_T(z)]dz + \int_{h/2}^{\tau/2}[P_G - P_T(z)]dz\right\} \tag{5}$$

Note that the liquid pressure appearing in Eq. (5) corresponds to that in the bulk-liquid reservoir. In effect, Eq. (5) replaces the inhomogeneous stress distribution by that in a homogeneous liquid slab exhibiting two zero-thickness interfaces in tension. Although others use differing designations [40,41,48,51,52], we label the term in braces as film tension, γ^f, or

$$\gamma^f \equiv \int_0^{h/2}[P_L - P_T(z)]dz + \int_{h/2}^{\tau/2}[P_G - P_T(z)]dz \tag{6}$$

With no loss in generality, the upper limit of the second integral may be replaced by infinity. The product of twice the film tension times film area A corresponds to the reversible work to increase film area at constant film thickness or

$$dW^{f}_{rev1} = 2\gamma^f dA \quad \text{constant } h \tag{7}$$

Film tension reduces exactly to the bulk liquid/gas surface tension, γ, in the limit of large film thickness where liquid and gas-reservoir pressures approach each other (i.e., where $P_G = P_L = P_N$)

$$\lim_{h\to\infty} 2\gamma^f = \int_{-\tau/2}^{+\tau/2}[P_N - P_T(z)]dz = \int_{-\infty}^{+\infty}[P_N - P_T(z)]dz \equiv 2\gamma \tag{8}$$

The factors of two appear so that an infinitely thick film displays two bulk surface tensions.

Surface tension in the film model is a function film thickness and corresponds to two zero-thickness membranes located in each half of the film. Fig. 7 illustrates force equivalence of the film model to the real system. Fig. 7a shows a schematic of the expected tangential-stress variation normal to the film [5,51] (see also Fig. 19). Because the film is thin, $P_T(z)$ does not attain the bulk gas stress at the film center. In Fig. 7b, two model membranes of tension are shown at positions $\pm z_f$. The film-model system in Fig. 7b consists of a bulk gas phase at pressure P_G surrounding the film, a bulk homogeneous liquid in the film at pressure P_L, and two zero-thickness membranes of tension at positions $\pm z_f$. We emphasize that liquid stress in the film model is that of the bulk liquid in the meniscus. This choice is demanded by the definition of area extension/contraction reversible work in Eqs. (5) and (6). Fig. 7b defines the film model.

Exact location of the two zero-volume tension membranes is not necessary to evaluate Eq. (6). Nevertheless, specifying where the membranes are located is important for complete mechanical equivalence. To establish that location (i.e., $\pm z_f$), we invoke equivalence of angular momentum about the z_f plane in the actual and model systems of Fig. 7 [64]

$$\int_0^{\tau/2}[z - z_f]P_T(z)dz = \int_0^{h/2}[z - z_f]P_L dz + \int_{h/2}^{\tau/2}[z - z_f]P_G dz \tag{9}$$

or after rearrangement and substitution of Eq. (6), we find that

$$z_f\gamma^f = \int_0^{h/2} z[P_L - P_T(z)]dz + \int_{h/2}^{\tau/2} z[P_G - P_T(z)]dz \tag{10}$$

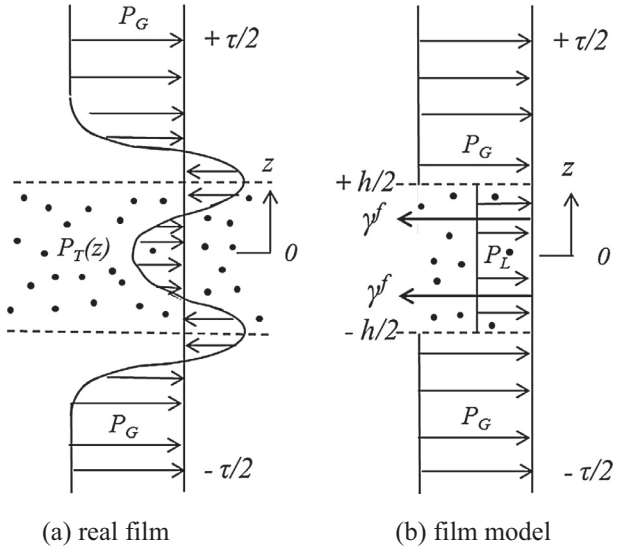

Fig. 7. Schematic of the transverse stress profile normal to the film. Dotted region locates the film. (a) Real system (see also Fig. 19). P_T does not attain the bulk gas value in the film. (b) Film-model system in which the tangential stress in the gas is uniform at P_G outside the film of thickness h and uniform in the liquid phase at P_L inside the film. Equivalence of the net force on the vertical plane gives rise to film surface tensions at $\pm z_\gamma$. Drawing is not to scale.

Thus, location of the film-tension membranes is related to the first moment of the excess-stress distribution across each half film. Once the tangential stress profile is established, Eq. (10) sets the film membrane-of-tension locations rigorously.

The second work exchange in the film model is depicted in Fig. 8. The right piston of the rectangular container in Fig. 6 is replaced by a fixed wall. Consider a reversible infinitesimal insertion of the gas-reservoir piston while simultaneously withdrawing the liquid-reservoir piston but maintaining constant total volumes of gas (that surrounding the film plus that in the gas reservoir) and liquid (that in the film plus that in the liquid reservoir). No fluid volumes change magnitude. The net result of this process is thinning of the film as film liquid recedes into the liquid reservoir. A reverse process can also be envisioned of injecting bulk liquid into the film from the liquid reservoir while withdrawing the gas-reservoir piston, but again maintaining constant total liquid and gas

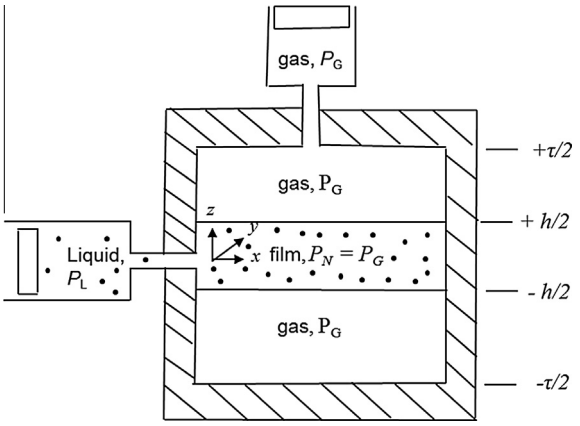

Fig. 8. A rectangular box of width w out of the paper and containing a free thin liquid film (shown dotted). The upper gas reservoir is connected to the gas below the film (not shown). $P_G > P_L$ due to terminating menisci (not shown). Gas is injected by infinitesimally depressing the gas-reservoir piston while liquid from the film is ejected by infinitesimally withdrawing the liquid-reservoir piston to reduce film thickness at constant film area. Drawing is not to scale.

volumes. It is clear that measurement of disjoining-pressure isotherms in the Scheludko or Mysels cells proceeds by the work process outlined in Fig. 8.

Differential isothermal work exchange done on the system in Fig. 8 is given by

$$dW^{f}_{rev2} = -P_G dV_{GR} - P_L dV_{LR} \quad \text{constant } T \tag{11}$$

where V_{GR} and V_{LR} are the volumes of the gas and liquid reservoirs, respectively. Because there is no compression or expansion of either phase, volumes of total liquid and gas are constant. Thus, for a constant-area change in film volume, we write that

$$dV_{GR} = -Ad(\tau - h) = Adh \quad \text{and} \quad dV_{LR} = -Adh \tag{12}$$

Combination of Eqs. (11) and (12) gives

$$dW^{f}_{rev2} = -(P_G - P_L)Adh \tag{13}$$

or from Eq. (2), we have that

$$dW^{f}_{rev2} = -\Pi Adh \tag{14}$$

We find that the measurement process of thickening or thinning the film in a Scheludko or Mysels' cell gives film reversible work in addition to the disjoining-pressure isotherm. Let the potential energy of the film or the disjoining potential, P_E, be defined by $\Pi \equiv -dP_E/dh$. Eq. (14) is then rewritten in integral form as

$$\frac{W^{f}_{rev2}}{A} = -\int_{\infty}^{h} \Pi(h')dh' = P_E(h) \quad \text{constant } A \tag{15}$$

where the film potential energy is zero at infinite thickness (i.e., corresponding to a bulk liquid phase exhibiting two bulk interfaces). The disjoining potential is equivalent to the reversible work per unit area necessary to thin the film from infinity to thickness h.

In summary, work exchange in the film model consists of two independent contributions corresponding to area change at constant thickness and thickness change at constant area or

$$dW^{f}_{rev} = dW^{f}_{rev1} + dW^{f}_{rev2} = 2\gamma^{f} dA - \Pi Adh \tag{16}$$

This result and the accompanying film-model schematic of Fig. 7b underpin film-model thermodynamics. Namely, all film-model thermodynamic properties are defined analogous to Eq. (6) as illustrated in Fig. 7b. That is, the actual inhomogeneous thin film exhibiting property density profiles is replaced by a hypothetical or model system consisting of a homogeneous continuous gas phase outside the film, a homogeneous bulk liquid phase of the same thickness and area as the film but consisting of thermodynamic properties identical to those in the liquid reservoir in equilibrium with the film, and surface excess properties located in two interfaces of zero thickness.

3.2. Membrane-model tension

Capillary work in the membrane model of a free thin liquid film is captured in Fig. 9. This figure is identical to Fig. 6 except that the liquid reservoir is eliminated. Menisci terminate the film but are not shown. Consider an infinitesimal withdrawal of the right piston while injecting gas from the reservoir while maintaining a constant total gas volume (i.e., reservoir plus container). Because no pressure–volume work is envisioned, film volume remains constant. This means that both film area and film thickness change during the work process: the film expands and thins such that the product Ah remains constant. Differential work for the reversible process in Fig. 9 is

$$dW^{m}_{rev3} = -2dA\int_{0}^{\tau/2} P_T(z)dz - P_G dV_{GR} \tag{17}$$

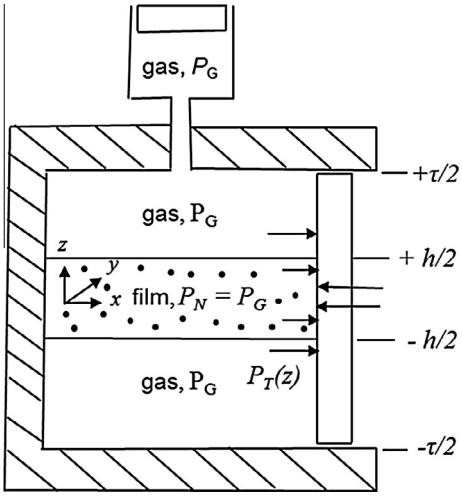

Fig. 9. A rectangular box of width w out of the paper and containing a free thin liquid film (shown dotted). The upper gas reservoir is connected to the gas below the film (not shown). $P_L \neq P_G$ due to terminating menisci (not shown). The right piston is infinitesimally translated to the right while the gas-reservoir piston is infinitesimally depressed while maintaining constant total gas and film volumes. Both film thickness and film area change at constant film volume. Drawing is not to scale.

But for constant film volume, we have that

$$dV_{GR} = -d[A(\tau - h)] = -\tau dA \tag{18}$$

Substitution of Eq. (18) into Eq. (17) gives the desired result

$$dW^{m}_{rev3} = 2dA\int_{0}^{\tau/2} [P_G - P_T(z)]dz \tag{19}$$

We identify the integral in Eq. (19) as the membrane tension

$$\gamma^{m} \equiv \int_{0}^{\tau/2} [P_G - P_T(z)]dz \tag{20}$$

Thus, in the membrane model, the actual transverse stress distribution is replaced by a single zero-thickness membrane of tension, as shown in Fig. 10. Liquid-film thickness, h, does not appear. Reversible work in the membrane model is then

$$dW^{m}_{rev3} = 2\gamma^{m} dA \tag{21}$$

No accounting is given for disjoining pressure because no liquid film exists in the membrane model, only vapor phase at pressure P_G and a zero-thickness membrane with tension $2\gamma^{m}$ (see Fig. 10b). The factor of 2 in the definition of membrane tension is consistent with the idea that as film thickness in Fig. 10a increases, two bulk interfaces are produced whose tensions are ascribed to a single zero-volume membrane.

Exact location of the membrane of tension, z_m, is established by equivalence of moments in the real and membrane-model systems. Following the same analysis as that in Eq. (9) for the film model, we find that $z_m = 0$ in obedience to symmetry. Again, location of the plane of membrane tension is immaterial to its evaluation. In the membrane model, however, the tension membrane (here of magnitude $2\gamma^{m}$) remains fixed at the center of the film even for thick films beyond the range of disjoining forces.

Comparison of Eqs. (6) and (20) along with Eq. (2) gives the oft-cited relation between film and membrane tensions [44–49,51,52]

$$2\gamma^{m} = 2\gamma^{f} + h(P_G - P_L) = 2\gamma^{f} + \Pi h \tag{22}$$

Film and membrane tensions both refer to zero-thickness membranes. They both depend on film thickness. They differ simply by the product of disjoining pressure and film thickness. However,

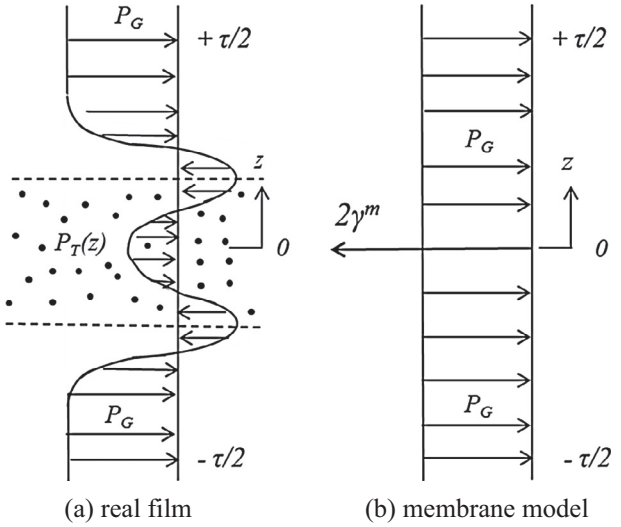

Fig. 10. Schematic of the transverse stress profile normal to the film. Dotted region locates the film. (a) Real system. P_T does not attain the bulk gas value in the film (see Fig. 19). (b) Membrane-model system in which the tangential stress in the gas is uniform at P_G throughout the container volume. Equivalence of the net force on the vertical plane gives rise to a single zero-thickness membrane surface tension at $z = 0$ of magnitude $2\gamma^m$. Drawing is not to scale.

their meanings are disparate. Film tension refers to a surface tension relative to a bulk liquid core of thickness h, whereas membrane tension, as defined here, does not require a film thickness for evaluation. There is no liquid phase in the membrane model.

As expected from Eq. (22), reversible capillary work expressions in the film and membrane models are related. It is straightforward to show that

$$dW^m_{rev3} = dW^f_{rev1} + dW^f_{rev2} \tag{23}$$

That is, the two work processes in Figs. 6 and 8 are encompassed in the single work process of Fig. 9 where film area and film thickness change simultaneously.

As with the film model, thermodynamic properties in the membrane model are defined analogous to Eq. (20) and illustrated in Fig. 10. Excess density (molar, energy, entropy, etc.) relative to that in the gas phase is integrated across the film and assigned to a zero-thickness membrane at z_m. Notably, film thickness does not appear.

3.3. Film-model thermodynamics

In the film model, a homogeneous slab of thickness h and with bulk-liquid properties replaces the region of density profiles. Upon allowing reversible heat and work exchange with the environment, including mass exchange, the first and second laws of thermodynamics for the gas/film system read

$$dU = TdS + 2\gamma^f dA - \Pi A dh - P_L dV_f - P_G dV_G + \sum_i \mu_i dn_i \tag{24}$$

where U, S, and n_i are container (gas plus liquid film) internal energy, entropy, and mole numbers of component i, respectively. μ_i is the chemical potential of component i, which along with temperature, is uniform throughout the system. The first term on the right of Eq. (24) describes reversible heat exchange while the remaining five terms reflect reversible work exchange. The second and third right factors correspond to reversible excess film work expressed in Eq. (16). Fourth and fifth terms account for reversible compression/expansion work of the homogeneous gas and liquid phases in the film-model system, whereas the last additive term on the right corresponds to reversible mass exchange. Note that the liquid pressure in term four corresponds to that in the film meniscus. Each extensive property is defined in terms of singlet density profiles. For example, the total system entropy is given by

$$S \equiv 2A\int_0^{+\tau/2} \tilde{s}(z)dz \tag{25}$$

where the over tilde indicates per unit volume so that $\tilde{s}(z)$ is the entropy density profile normal to the film (i.e., entropy per unit volume), and likewise for U and n_i.

Corresponding expressions for the differential internal energy of the homogeneous gas and liquid phases, respectively, are

$$dU_G = TdS_G - P_G dV_G + \sum_i \mu_i dn_i^G \tag{26}$$

and

$$dU_L = TdS_L - P_L dV_f + \sum_i \mu_i dn_i^L \tag{27}$$

Subtraction of Eqs. (26) and (27) from Eq. (24) gives the excess film differential internal energy

$$dU^f = TdS^f + 2\gamma^f dA - \Pi A dh + \sum_i \mu_i dn_i^f \tag{28}$$

where U^f is the total excess internal energy of the film located at the two film-model interfaces and is defined by

$$\begin{aligned} U^f &= U - U_L - U_G \\ &= 2A\left[\int_0^{h/2} [\tilde{u}(z) - \tilde{u}_L]dz + \int_{h/2}^{+\tau/2} [\tilde{u}(z) - \tilde{u}_G]dz\right] \equiv 2Au^f \end{aligned} \tag{29}$$

The liquid internal energy density, $\tilde{u}_L$ in Eq. (29), is that of the bulk-meniscus liquid in equilibrium with the film. The last identity in Eq. (29) defines excess interfacial internal energy per unit area, u^f, for each of the two film-model interfaces. Similarly, all extensive film-model properties are defined analogous to Eqs. (6) and (29). Thus, film interface excess entropy is

$$\begin{aligned} S^f &= S - S_L - S_G \\ &= 2A\left[\int_0^{h/2} [\tilde{s}(z) - \tilde{s}_L]dz + \int_{h/2}^{+\tau/2} [\tilde{s}(z) - \tilde{s}_G]dz\right] \equiv 2As^f \end{aligned} \tag{30}$$

and, in particular, component i excess moles of the two interfaces is

$$n_i^f = 2A\left[\int_0^{h/2} [\rho_i(z) - \rho_i^L]dz + \int_{h/2}^{+\tau/2} [\rho_i(z) - \rho_i^G]dz\right] \equiv 2A\Gamma_i^f \tag{31}$$

The far-right identity in Eq. (31) defines the adsorption (moles per unit area) of component i per interface of the film and is symbolized by Γ_i^f. Again, component i liquid density appearing in the first integral of Eq. (31) is that of the bulk liquid in the film meniscus.

Fig. 11 illustrates the meaning of film-model excess adsorption. A solvent density profile (e.g., water) is shown on the left for a thin liquid film where $\rho_1(z)$ is the local molar density of the solvent. This density profile is replaced in the film model by a slab of solvent at the bulk liquid reservoir density, ρ_1^L, surrounded by homogeneous equilibrium vapor at bulk density, ρ_1^G. Once film thickness is specified, excess mass is attributed to two zero-volume planes located at $\pm h/2$. Note in Fig. 11a that the solvent bulk liquid density nowhere appears in the actual film. As discussed above, ρ_1^L and ρ_1^G are not the densities on the bimodal-phase envelop since the pressure in the meniscus liquid is not that of the gas phase. In the limit of an infinitely thick film, Γ_i^f becomes the Gibbsian excess mass or adsorption of component i at a single liquid/gas interface [78].

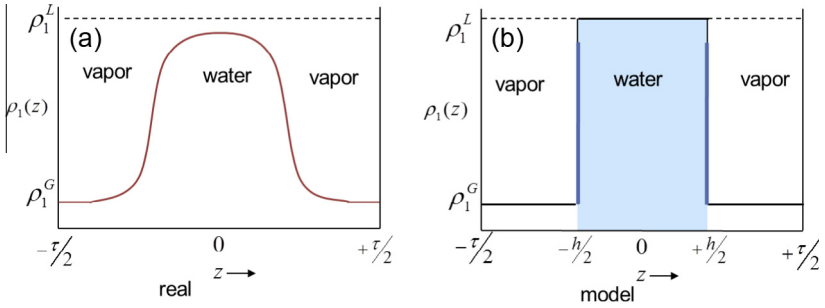

Fig. 11. Schematic of real and film-model systems for solvent density in a free thin liquid film. (a) The actual density distribution is replaced in (b) by a slab of density corresponding to the bulk liquid reservoir. Excess mass, positive or negative, is attributed to two zero-volume planes at ±h/2 (gray vertical solid lines).

To establish the film-model excess internal energy, Eq. (28) is integrated at constant intensive properties of T, h, and μ_i [48,51,78–80] or

$$U^f = TS^f + 2\gamma^f A + \sum_i \mu_i n_i^f \tag{32}$$

The process of integrating Eq. (28) is equivalent to assembling a larger film from smaller ones by Euler's rule. This requires the smaller films to be of identical intensive properties including thickness so that the disjoining pressures are identical. As noted above in Section 2.2, the disjoining-pressure isotherm is a material property further accentuating that film thickness is an intensive variable.

Many interfacial thermodynamic free energies may be defined as convenience dictates. For example, film-model excess Helmholtz free energy, F^f, is defined as

$$F^f/2A = f^f \equiv u^f - Ts^f = \gamma^f + \sum_{i=1}^{c} \mu_i \Gamma_i^f \tag{33}$$

If no components adsorb, then the film-model Helmholtz excess free energy per unit area, F^f/A, is equivalent to twice the film surface tension. This case arises for a single component in the Gibbs zero-solvent-adsorption convention, as discussed below.

3.4. Film-model Gibbs adsorption equation

Following classical procedures [64,81–83], differentiation of Eq. (32) followed by comparison to Eq. (28) reveals that [78,79]

$$-d\gamma^f = s^f dT + \Pi dH + \sum_{i=1}^{c} \Gamma_i^f d\mu_i \tag{34}$$

where $H = h/2$ is the half thickness of the film. This expression is an analogue of the Gibbs adsorption equation for a single interface [63,64,78,82,83]. Unfortunately, Eq. (34) is over specified [64,78]. It indicates that film tension is a function of $c + 2$ variables, whereas the phase rule accounting for the curved meniscus demands $c + 1$ independent variables [63,64]. To relieve this inconsistency, we combine the Gibbs–Duhem equations for the bulk liquid and gas phases as follows

$$\Delta\tilde{s}dT + dP_C + \sum_{i=1}^{c} \Delta\rho_i d\mu_i = 0 \tag{35}$$

where the operator Δ indicates the difference between liquid and gas (e.g., $\Delta\tilde{s} \equiv \tilde{s}_L - \tilde{s}_G$). Thus, of the $c + 2$ system variables only $c + 1$ are independent. Elimination of the solvent chemical potential, μ_1, between Eqs. (34) and (35) and implementation of the definition of disjoining pressure in Eq. (2) give

$$-d\gamma^f = \left[s^f - \Gamma_1^f \frac{\Delta\tilde{s}}{\Delta\rho_1}\right] dT + \left[\Pi - \Gamma_1^f \frac{d\Pi/dH}{\Delta\rho_1}\right] dH + \sum_{i=2}^{c} \left[\Gamma_i^f - \Gamma_1^f \frac{\Delta\rho_i}{\Delta\rho_1}\right] d\mu_i \tag{36}$$

Film tension in Eq. (36) is now correctly a function of $c + 1$ independent thermodynamic variables. Appendix A demonstrates that the coefficients multiplying temperature and chemical-potential differentials in Eq. (36) are independent of the choice of film thickness (i.e., they are Gibbs invariants [64,78,83]). However, the coefficient of the thickness variable is not. Apparently, this means that film tension is not a thermodynamic measureable property, but rather is model dependent. One resolution is to change variables in Eq. (36), for example, by subtracting the term $d(\Pi H)$ from both sides

$$-d(\gamma^f + \Pi H) \equiv -d\gamma^m = \left[s^f - \Gamma_1^f \frac{\Delta\tilde{s}}{\Delta\rho_1}\right] dT - \left[H + \frac{\Gamma_1^f}{\Delta\rho_1}\right] d\Pi + \sum_{i=2}^{c} \left[\Gamma_i^f - \Gamma_1^f \frac{\Delta\rho_i}{\Delta\rho_1}\right] d\mu_i \tag{37}$$

Here all coefficients of the independent differential variables are Gibbs invariants. That is, they do not depend on the precise location of the film-model dividing surfaces, meaning that the quantity $\gamma^f + \Pi H$ is thermodynamically well defined. As the first equality in Eq. (37) indicates, $\gamma^f + \Pi H$ is the membrane tension γ^m (compare Eq. (22)). We conclude that membrane tension is a Gibbs invariant [64,78,83].

Nevertheless, Eq. (36) is useful when, following Gibbs [64,78,83], we set the film thickness corresponding to zero adsorption of component 1, typically the solvent.

$$\Gamma_1^f = \int_0^{h_1/2} [\rho_1(z) - \rho_1^L] dz + \int_{h_1/2}^{+\tau/2} [\rho_1(z) - \rho_1^G] dz = 0 \tag{38}$$

This convention is appealing because, for thick films, it coincides with the classic Gibbs convention [62–65,67,78,82,83]. Fig. 12 illustrates calculation of the two film-model dividing surfaces at $\pm h_1/2 = \pm H_1$ according to Eq. (38). Mole densities of the bulk solvent gas and liquid phases are extrapolated to the dividing surfaces such that the cross-hatched areas above solvent density profile up to the liquid density equal those below the solvent density profile down to the gas density. Upon multiplying Eq. (38) by 2 and re-expressing the various integrals gives [48,51]

$$h_1 = \frac{n_1/A - \rho_1^G \tau}{\Delta\rho_1} \tag{39}$$

where n_1 is the total moles of solvent in the system. Eq. (39) is commonly adopted in molecular simulations of disjoining pressures in free thin liquid films [60,84,85].

Fig. 13 illustrates how the zero-solvent-adsorption convention applies to component adsorption. A schematic molar-density profile is highlighted for a somewhat surface-active, low volatility aqueous solute (such as a higher molecular-weight alcohol). The alcohol preferentially partitions near the two film interfaces but does not attain the bulk-component liquid density in the film core

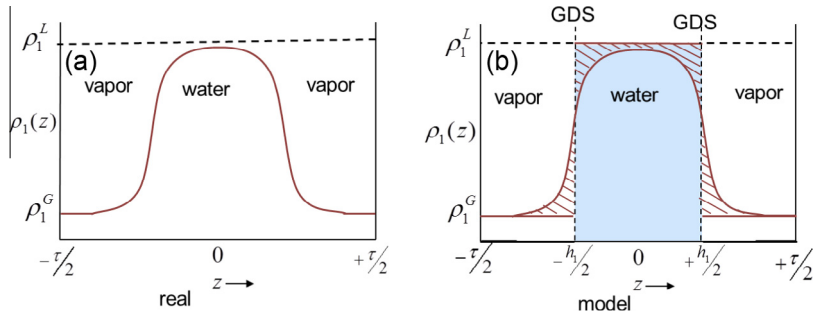

Fig. 12. Schematic for constructing film thickness according to Gibbs convention in the film model. (a) Real system. (b) Film-model system in which adsorption of solvent is zero at each dividing surface. Illustrated areas above and below the solvent density profile are equal specifying h_1. The liquid density adopted in the film-thickness calculation is that of the bulk liquid meniscus.

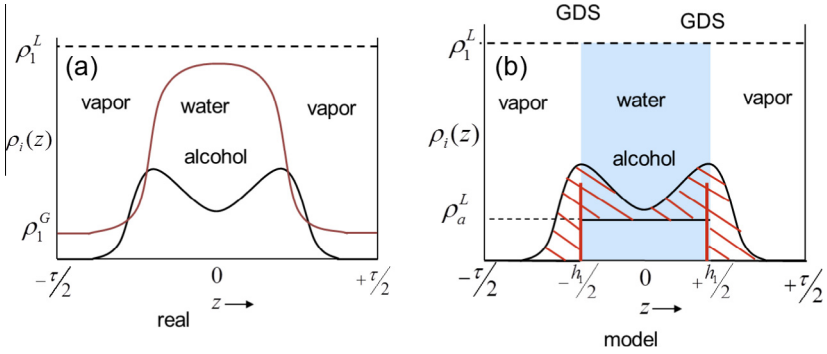

Fig. 13. Schematic for determining component adsorption (e.g., alcohol) according to Gibbs convention in the film model. (a) Real system. (b) Model system in which adsorption of solvent is zero at each dividing surface, $\pm h_1/2$. Illustrated areas in (b) establish alcohol adsorption which is attributed to the two zero-thickness dividing surfaces. Liquid-component molar density employed for calculation is that of the bulk liquid meniscus.

corresponding to that in the meniscus. Alcohol film-model adsorption at each interface, symbolized by Γ^f_{a1}, is given by

$$\Gamma^f_{a1} = \int_0^{h_1/2} [\rho_a(z) - \rho^L_a]dz + \int_{h_1/2}^{+\tau/2} [\rho_a(z) - \rho^G_a]dz \tag{40}$$

Thus in Fig. 13b, bulk gas and liquid alcohol densities are extrapolated to the dividing surfaces at $\pm h_1/2$, and the cross-hatched areas are calculated. All excess moles of alcohol are then assigned to the two zero-thickness dividing surfaces, shown by the gray solid vertical lines at $\pm h_1/2$ in Fig. 13b.

We designate film-model thermodynamic properties based on a thickness corresponding to zero-solvent adsorption (i.e., based on setting the location of the two interface dividing surfaces at $\pm h_1/2$ in Fig. 13) with a unity subscript. All excess thermodynamic properties follow as in Eqs. 29–31, but with h replaced by h_1. According to this Gibbs-motivated convention, Eq. (36) transforms to

$$-d\gamma^f = s^f_1 dT + \Pi dH_1 + \sum_{i=2}^{c} \Gamma^f_{i1} d\mu_i \tag{41}$$

Film tension remains a function of $c + 1$ independent variables, but now all coefficients are carefully defined. Eq. (41) is the film-model Gibbs adsorption equation: an analogue of the Gibbs adsorption equation for single interfaces. As film thickness increases beyond the range of thin-film forces, Eq. (41) reduces to the classic Gibbs adsorption equation [64,78,83].

Since film tension is not directly measureable, the film-model Gibbs adsorption equation is not as useful as is the Gibbs adsorption equation. Nevertheless, it is a helpful result. Following others [6,79,80], the disjoining-pressure isotherm can be established from the thickness dependence of component adsorption. Cross-differentiation of Eq. (41) gives

$$\left(\frac{\partial \Pi}{\partial \mu_i}\right)_{T,h_1,\mu_{j\neq i,1}} = \left(\frac{\partial \Gamma^f_{i1}}{\partial H_1}\right)_{T,\mu_{i\neq 1}} \tag{42}$$

This result may be integrated to quantify the contribution of dissolved solutes to disjoining pressure

$$\Pi(h_1) - \Pi^o(h_1) = 2R_g T \sum_{i=2}^{c} \int_0^{a_i} \left(\frac{\partial \Gamma^f_{i1}}{\partial h_1}\right) d\ln a_i \quad \text{constant} \quad T, h_1, a_{j\neq i,1} \tag{43}$$

where Π^o denotes the disjoining pressure of pure solvent, R_g is the ideal-gas constant, and a_i is the activity of component i. For an ideal aqueous alcohol solution, the alcohol contribution to the disjoining-pressure isotherm follows as

$$\Pi(h_1) - \Pi^o(h_1) = 2R_g T \int_0^{x_a} \left(\frac{\partial \Gamma^f_{i1}}{\partial h_1}\right) d\ln x_a \quad \text{constant } T, h_1 \tag{44}$$

where x_a is the mole fraction of alcohol in the aqueous liquid meniscus. If theory or experiment is available for how solute adsorption changes with film thickness at given bulk concentration, Eq. (44) establishes the solute contribution to the disjoining-pressure isotherm. Considerable effort has been focused on this approach, especially for confined films [79,86–94].

The pure liquid/vapor disjoining pressure, Π^o, is often expressed in terms of the equilibrium fugacity (or pressure) in the gas phase surrounding the film. Although pressures in the liquid meniscus and vapor phase are different, their chemical potentials are identical (i.e., $\mu_G = \mu_L \equiv \mu$). Integration of Gibbs–Duhem equations for the bulk liquid and gas phases specifies that

$$\mu - \mu^{sat} = \int_{P^{sat}}^{P_L} v_L dP = \int_{P^{sat}}^{P_G} v_G dP \quad \text{constant} \quad T \tag{45}$$

where v is molar volume, and superscript *sat* indicates the saturated phase equilibrium for a planar interface. Eq. (45) is particularly useful in molecular simulation of single-component free thin liquid films for it establishes the disjoining pressure for a simulated film of given thickness [60,84]. It is restricted to a pure component. For an incompressible liquid, the first right equality is re-expressed as $v_L^{sat}(P_G - P^{sat} - \Pi^o) = \mu - \mu^{sat} = R_g T \ln f_G/f^{sat}$. Rewriting this result gives

$$\Pi^o(h_1) = -\rho_L^{sat} R_g T \ln f_G/f^{sat} - (P^{sat} - P_G) \quad \text{constant } T \tag{46}$$

where f denotes fugacity [95]. The second term on the right of this expression is commonly neglected [6]. Eq. (46) bares strong resemblance to that of Kelvin for vapor-pressure lowering of a vapor bubble [63,64]. As above, let C_m denote the mean curvature in the bulk meniscus designated positive on the concave (gas) side of the interface. Substitution of the rigorous form of Kelvin's equation then yields

$$\Pi^o(h_1) = 2\gamma C_m \equiv P_C \tag{47}$$

The second equality follows from the Young–Laplace equation and confirms the consistency of the definition of disjoining pressure in Eq. (2). Eqs. (46) and (47) reveal that the gas phase over a free liquid thin film is conceptually identical to that inside an isolated vapor bubble. As the film thins for a positive, negative-sloped disjoining-pressure isotherm, meniscus curvature increases reflecting an increase in capillary pressure.

A second important result from the film-model Gibbs adsorption equation is calculation of film tension from the measured disjoining-pressure isotherm. Integration of Eq. (41) gives

$$2\gamma^f(h_1) = 2\gamma - \int_{\infty}^{h_1} \Pi(h_1')dh_1' \quad \text{constant } T,\ \mu_{i\neq 1} \tag{48}$$

or from Eq. (15), we have that

$$2\gamma^f(h_1) = 2\gamma + P_E(h_1) \quad \text{constant } T,\ \mu_{i\neq 1} \tag{49}$$

Accordingly, film tension equals the bulk liquid/gas surface tension plus one-half the disjoining potential of the film, which is a function of film thickness. This result allows the film-model Helmholtz excess free energy to be written as

$$2f^f = 2\gamma + P_E(h_1) + 2\sum_{i=2}^{c} \Gamma_{i1}^f \mu_i \tag{50}$$

An even more simple and appealing result emerges for a single-component film

$$2f^f = 2\gamma + P_E(h_1) \tag{51}$$

Film-model Helmholtz excess free energy is the film surface tension plus one-half the film disjoining potential. This result is often invoked intuitively, although the zero-solvent-adsorption thickness convention is not emphasized [96].

3.5. Membrane-model thermodynamics

In the membrane model, the combined first and second law for the film/gas system is written analogous to that for the film model in Eq. (24) but now consonant with the definition of membrane tension depicted in Fig. 10b

$$dU = TdS + 2\gamma^m dA - P_G dV + \sum_i \mu_i dn_i \tag{52}$$

where V is the entire volume of the container. In this expression, disjoining pressure is absent consistent with the definition of membrane tension in Eq. (20) and capillary work in Eq. (21). Pressure–volume work for a liquid phase is also missing because only a bulk gas phase and a zero-thickness membrane are present in the membrane-model system. Consequently, the container system constitutes a bulk gas occupying total container volume plus a zero-volume membrane (i.e., $U = U_G + U^m$). Eq. (26) holds (with the bulk gas phase occupying the entire container volume) giving the membrane differential excess internal energy as

$$dU^m = TdS^m + 2\gamma^m dA + \sum_i \mu_i dn_i^m \tag{53}$$

where U^m is the total excess internal energy of the membrane defined by

$$U^m = U - U_G = 2A\int_0^{\tau/2} [\tilde{u}(z) - \tilde{u}_G]dz \equiv 2Au^m \tag{54}$$

Again no liquid-phase properties appear. The factor of 2 in Eq. (54) is convenient for comparison to film-model thermodynamic properties. Other membrane-model properties are defined analogously. For example, membrane excess entropy and excess component mole numbers read

$$S^m = S - S_G = 2A\int_0^{\tau/2} [\tilde{s}(z) - \tilde{s}_G]dz \equiv 2As^m, \tag{55}$$

and

$$n_i^m = 2A\left[\int_0^{\tau/2} \left[\rho_i(z) - \rho_i^G\right]dz\right] \equiv 2A\Gamma_i^m \tag{56}$$

As pictured in Fig. 14, component adsorption includes the entire moles in the film in excess of the gas phase. No film thickness need be specified to determine excess membrane-model properties. Fig. 15 illustrates the meaning of membrane-model adsorption. Excess component moles over that of the gas are lumped into a zero-thickness surface. Where the surface of excess moles is located is immaterial, since thermodynamic properties in the membrane model do not require a film thickness. For thick films, membrane-model adsorption does not reduce to the Gibbs adsorption for each bulk interface but includes the bulk moles distributed across the film core. From the definitions of excess surface moles in the film and membrane models (compare Eqs. (31) and (56)), we find that

$$\Gamma_i^m = \Gamma_i^f + H\Delta\rho_i \tag{57}$$

where H is, again, the film half thickness. This expression is analogous to Eq. (22) relating membrane tension and film tension. Other thermodynamic properties of the two thin-film models are similarly related, such as entropy

$$s^m = s^f + H\Delta\tilde{s} \tag{58}$$

Various excess free energies in the membrane model follow similar definitions as in Eqs. (54)–(56) and can be similarly related to those in the film model.

3.6. Membrane-model Gibbs adsorption equation

Eq. (53) is integrated at constant intensive variables to give

$$U^m = TS^m + 2\gamma^m A + \sum_i \mu_i n_i^m \tag{59}$$

This result is closely allied to Eq. (32), but the meaning of the superscripted variables is quite different. In the membrane model, no film thickness is invoked. Differentiation of Eq. (59) and comparison to Eq. (53) gives the membrane-model analogue of the Gibbs adsorption equation

$$-d\gamma^m = s^m dT + \sum_{i=1}^{c} \Gamma_i^m d\mu_i \tag{60}$$

which correctly specifies membrane tension as a function of $c + 1$ intensive variables. By definition, the coefficients of differential

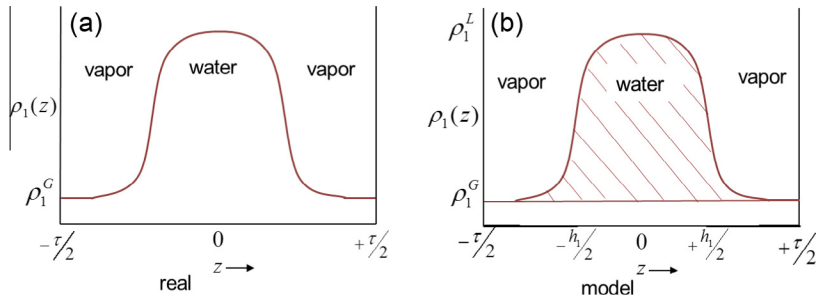

Fig. 14. Schematic for constructing the excess component moles in the membrane-model system. (a) Real system. (b) Membrane-model system in which adsorption of solvent is reflected by the area of the under the density profile and over the bulk gas density. There is no dividing surface.

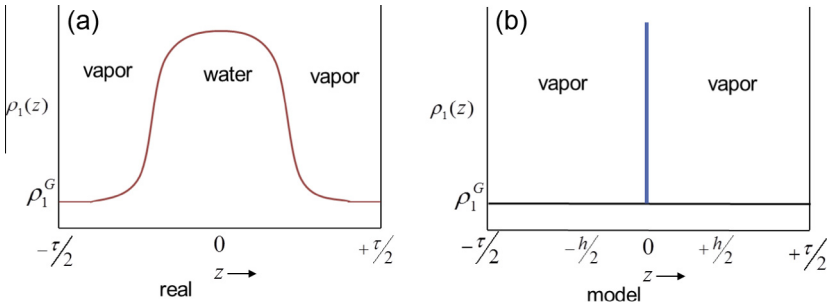

Fig. 15. Schematic of real (a) and membrane-model system (b) for solvent molar density in a free thin liquid film. Excess moles defined in Fig. 14 (b) are collapsed to a membrane of zero thickness surrounded by vapor (gray vertical solid line in b). Exact location of the membrane is immaterial.

temperature and chemical potential are well-defined Gibbs invariants. They do not involve film thickness. Unfortunately, no explicit information is available for disjoining forces as in Eq. (34) of the film model. Elimination of the solvent chemical potential in Eq. (60) in favor of capillary pressure from Gibbs–Duhem in Eq. (35) provides that information

$$-d\gamma^m = \left[s^m - \Gamma_1^m \frac{\Delta\tilde{s}}{\Delta\rho_1}\right]dT - \frac{\Gamma_1^m}{\Delta\rho_1}d\Pi + \sum_{i=2}^{c}\left[\Gamma_i^m - \Gamma_1^m\frac{\Delta\rho_i}{\Delta\rho_1}\right]d\mu_i \quad (61)$$

Again, all coefficients of the differentials on the right are Gibbs invariants. As opposed to the film model, it is not possible to set $\Gamma_1^m = 0$. Substitution of Eqs. (57) and (58) (i.e., the relations between membrane and film-model properties) exactly reproduces Eq. (37). This exercise proves the consistency of the two thermodynamic models.

Although the membrane model does not invoke film thickness, the second term on the right of Eq. (61) motives an apparent thickness defined by

$$H_m = h_m/2 \equiv \frac{\Gamma_1^m}{\Delta\rho_1} \quad (62)$$

With this convention and with the definition of film potential energy in Eq. (15), integration of Eq. (61) yields

$$2\gamma^m = 2\gamma + \Pi h_m + P_E(h_m) \quad \text{constant } T,\ \mu_{i\neq 1} \quad (63)$$

Substitution of the relation between membrane and film tension, Eq. (22), shows that

$$2\gamma^f(h_m) = 2\gamma + P_E(h_m) \quad \text{constant } T,\ \mu_{i\neq 1} \quad (64)$$

This result is consistent with but not identical to Eq. (49). The distinction arises because film potential energy is evaluated at h_m rather than h_1 in Eq. (49). As confirmed in Fig. 20 below, small differences in the exact definition of film thickness for evaluating disjoining forces are most likely not of practical import especially since experimental film thicknesses are almost always optical in origin.

Finally analogous to Eq. (33), excess film Helmholtz free energy in the membrane model is given by

$$F^m/2A = f^m \equiv u^m - Ts^m = \gamma^m + \sum_{i=1}^{c}\mu_i\Gamma_i^m \quad (65)$$

which is identical in form to Eq. (33) except the superscripted terms have different definitions.

3.7. Meniscus profile

Meniscus shape is couched only in the film model. In this section, we adopt Gibbs' zero-solvent-adsorption convention and discard the subscript unity on film half thickness so that $H = h_1/2$. The goal is to predict the meniscus profile, $H(x)$, from the film lateral center into the meniscus as depicted in Fig. 16. Film half thickness at $x = 0$ is H_f. The meniscus triple line terminates at $x = L$ with half thickness H_L and with a solid/liquid/gas equilibrium contact angle of θ. Container walls are diathermal; menisci are presumed sufficiently large such that small changes in film volume and area do not alter meniscus composition.

Since temperature, volume, solid-container surface area, and component chemical potentials are constant, it is convenient to introduce the grand-potential free energy: $\Omega \equiv U - TS - \sum_{i=1}^{c}\mu_i n_i$. Euler integration of Eq. (24), including surface energies of the solid/liquid and solid/gas interfaces, gives

$$\Omega = -P_G V_G - P_L V_L + 2\gamma^f A^{LG} + 2\gamma^{SL}A^{SL} + 2\gamma^{SG}A^{SG} \quad (66)$$

where volume V_L and liquid/gas surface half-area A^{LG} correspond to those exhibited by the film plus the meniscus region. Superscripts *SL* and *SG* denote the solid/liquid and solid/gas container interfaces. Factors of 2 arise because areas correspond to half of the film. The bulk liquid pressure in the meniscus appears (as opposed to the normal stress of the film) consistent with the thermodynamic definition of film tension in Eq. (6). Similarly, disjoining pressure does not appear in Eq. (66) because film thickness is an intensive variable. Film tension is recognized as a function of film thickness,

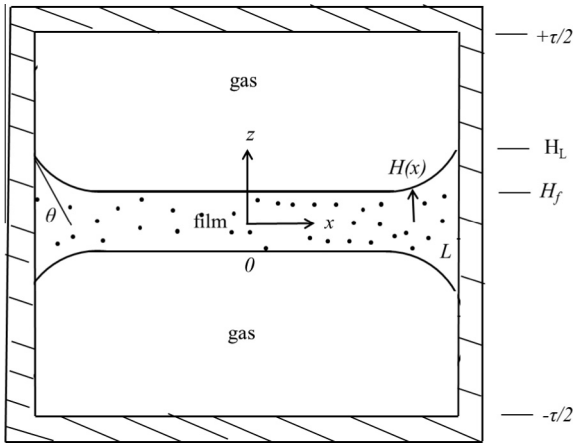

Fig. 16. Schematic of thin film in the rectangular container of Figs. 2 and 3 with attached meniscus. Film upper-interface profile, $H(x)$, is labeled. Drawing is not to scale.

and possibly other thickness characteristics such as the square of the profile slope [97,98]. Here, we treat γ^f as a function of film thickness only, neglecting higher-order contributions [99,100].

Evaluation of volumes and areas in Eq. (66) is presented in Appendix B. Let w represent container width in Fig. 16. The grand potential then becomes

$$\Omega = -P_C 2w\tau L + 4wP_C\int_0^L H(x)dx + 4w\int_0^L \gamma^f\sqrt{1+H_x^2}dx + \gamma^{SG}2w\tau + (\gamma^{SL}-\gamma^{SG})4wH_L \tag{67}$$

Subscript x on film half thickness indicates a derivative. The grand potential is an extremum for differential changes about equilibrium at constant temperature, container volume and area, and component chemical potentials. Thus, we desire that particular meniscus profile, $H(x)$, that extremizes grand free energy [19,97–103]. Accordingly, we functionally differentiate Eq. (67) as

$$0 = \delta\int_0^L\left[\gamma^f\sqrt{1+H_x^2}+P_C H\right]dx + (\gamma^{SL}-\gamma^{SG})\delta H_L \tag{68}$$

where δ denotes functional differentiation. Constraints are fixed film half thickness at $x = 0$ and fixed contact angle at $x = L$. As demonstrated in Appendix B, performing the functional differentiation yields two independent equilibrium relations

$$\gamma\cos\theta = \gamma^{SG} - \gamma^{SL} \tag{69}$$

and

$$\gamma^f\frac{H_{xx}}{(1+H_x^2)^{3/2}} - \left(\frac{d\gamma^f}{dH}\right)\frac{1}{(1+H_x^2)^{1/2}} - P_C = 0 \tag{70}$$

The first condition, Eq. (69), is the classic Young–Dupré solid/liquid/gas contact-angle condition [62–64]. Eq. (70), however, is a new result. Following Deryagin and coworkers [4–6], we assume that Eq. (49) holds locally even though film thickness varies. Substitution of Eq. (49) into Eq. (70) gives a modified Young–Laplace equation allowing calculation of film profiles

$$\left[\gamma+\frac{1}{2}P_E(h_1)\right]\frac{H_{xx}}{(1+H_x^2)^{3/2}} + \Pi(h_1)\frac{1}{(1+H_x^2)^{1/2}} = P_C \tag{71}$$

Eq. (71) correctly reduces to that of Young and Laplace in the film meniscus where film thickness is large and disjoining forces vanish

$$\gamma\frac{H_{xx}}{(1+H_x^2)^{3/2}} = 2\gamma C_m = P_C \quad \text{meniscus} \tag{72}$$

In the flat portion of the film where H_x and H_{xx} vanish and disjoining forces dominate, the definition of disjoining pressure in Eq. (2) correctly emerges

$$\Pi(h_1) = P_C \quad \text{flat film} \tag{73}$$

Nevertheless, the classic augmented Young–Laplace equation of Deryagin [4,6,45–47,97,98,104]:

$$\gamma\frac{H_{xx}}{(1+H_x^2)^{3/2}} + \Pi(h_1) = P_C, \tag{74}$$

is not reproduced exactly. Quantitative difference between the modified and augmented Young–Laplace equations, however, is not significant. In the meniscus region, $P_E < \gamma$, and Π vanishes. In the flat portion of the film, profile curvature and slope do not contribute. Still, the modified Young–Laplace equation is not an ansatz. It arises directly from the thermodynamic formulation presented in Section 3.3. Extension of Eqs. (71) and (74) to cylindrical films is straightforward [97,98].

In the membrane model, no film thickness directly appears. Rather, the single zero-thickness film membrane intersects the bulk meniscus discontinuously at a film/meniscus contact line. There is no analogous augmented Young–Laplace equation. Nevertheless, a finite contact angle at the contact line does result as outlined below.

3.8. Film contact angle

3.8.1. Film model

Thin-film forces distort the meniscus profile from that of constant curvature. For this reason, the continuous film-thickness profile appears to intersect the flat portion of the film with a finite contact angle, θ_f, illustrated in Fig. 17. In the film model, the film contact angle is conveniently defined as that extrapolated from the constant-curvature portion of the meniscus to the film midplane at $z = 0$ [4,6,48,52,97,98,104] An expeditious route to establish θ_f is through an equilibrium force balance on the film as portrayed in Fig. 17. Bulk liquid pressure appears in the balance even though P_L does not actually exist in the thin film. Appearance of P_L is demanded by the definition of film tension in Eqs. (6) and (66).

As outlined in Appendix C, resolution of x-forces in Fig. 17 gives

$$\gamma^f(H)\cos\varphi(H) = \gamma^f(H_f) + \Pi(H_f)H_f - P_C H \tag{75}$$

where φ is the local angle between the profile tangent and the horizontal and H is the local half-film thickness defined in the Gibbs convention of Eq. (38). Far into the meniscus where film thickness is large, film tension becomes the bulk surface tension, γ, so that Eq. (75) reduces to

$$\gamma\cos\varphi(H) = \gamma^f(H_f) + \Pi(H_f)H_f - P_C H, \quad H \text{ large} \tag{76}$$

Hence, the cosine of the local angle φ is linear in H for large film thickness. Evaluation of the intercept in Eq. (76) conveniently gives the film contact angle

$$\gamma\cos\theta_f = \gamma^f(H_f) + \Pi(H_f)H_f \tag{77}$$

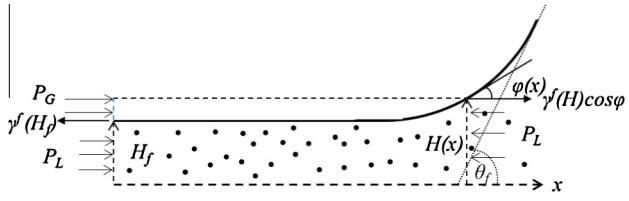

Fig. 17. Control volume enclosed in dashed lines for x-force balance on a free liquid thin film shown dotted. x-Tension and pressure forces acting on the control volume are indicated by arrows. The local tangent angle with the horizontal axis is φ, while the macroscopic contact angle of the film is θ_f. Resolution of z-forces is by film symmetry.

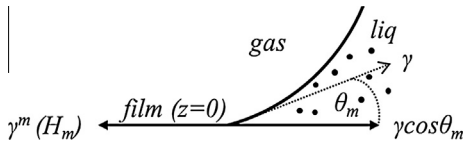

Fig. 18. Schematic of x-force balance for the upper half of the membrane model. The film is pictured as a zero-thickness membrane located at the film midplane which meets the bulk liquid meniscus (shown dotted) with a finite contact angle θ_m. Resolution of z-forces is by film symmetry.

Substitution of Eq. (48) gives the desired result

$$\cos\theta_f = 1 + \frac{1}{2\gamma}\left[\Pi(h_f)h_f + \int_{h_f}^{\infty}\Pi(h_1')dh_1'\right] = 1 + \frac{1}{2\gamma}\int_0^{\Pi(h_f)} h_1(\Pi')d\Pi' \tag{78}$$

where h_f is the film-model zero-solvent-adsorption film thickness in the flat region. The factor of 2 arises from the symmetry of the film. This expression is well cited, especially when written for wetting/adsorbed solid-supported liquid films [6,46,47,51,57,63,104–106] as the Frumkin/Deryagin relation [4,5,59]. A deep attractive minimum must be present in the disjoining-pressure isotherm to produce finite film contact angles.

Eq. (78) can also be derived from the augmented Young–Laplace equation, Eq. (74), by reduction-of-order integration to specify H_x [98,99]. Because $\cos\varphi = 1/\sqrt{1+H_x^2}$, Eq. (76) emerges from this analysis at large film separations. Eq. (78) follows [98,99]. Appendix D demonstrates that the modified Young–Laplace equation, Eq. (71), also yields the Frumkin–Deryagin expression for the film contact angle.

3.8.2. Membrane model

In the membrane model, there is no film profile only gas and a zero-volume membrane. Nevertheless, a film contact angle can be defined. As shown in Fig. 18, the bulk meniscus meets the zero-thickness membrane of tension with a finite contact angle θ_m. An x-force balance performed near the contact line is illustrated in Fig. 18

$$\gamma\cos\theta_m = \gamma^m(H_m) \tag{79}$$

where H_m is the apparent half-film thickness defined in Eq. (62). Substitution of Eqs. (15) and (63) reveals that

$$\cos\theta_m = 1 + \frac{1}{2\gamma}\int_0^{\Pi(h_m)} h_m(\Pi')d\Pi' \tag{80}$$

This result is identical in form to Eq. (78), strengthening the consistency of the two thermodynamic models. However, there is a subtle difference. The film thicknesses at which disjoining pressures are evaluated are slightly different, similar to Eqs. (49) and (64) discussed above.

4. Theory

4.1. Square-gradient theory (SGT)

Perhaps the simplest theory to illustrate the properties of thin liquid films is that of van der Waals [65,67,107] later referred to as Cahn–Hilliard [108] and/or square-gradient theory (SGT) [67]. In van der Waals' picture of an interface for a single component, the local free-energy density profile consists of a homogeneous free energy evaluated at the local molar density and a second term to account for local gradients in molar density. The correction term for density inhomogeneity is proportional to the density gradient squared (i.e., to ρ_z^2). This formulation leads to a spatially uniform chemical potential, μ, as the sum of two terms

$$\mu = \mu_o(\rho) - c\rho_{zz} \quad \text{constant } T \tag{81}$$

where μ_o is the chemical potential of a homogeneous fluid evaluated at the local density and c is the influence parameter taken here as constant. Given an appropriate equation of a state (EOS) to specify μ_o (and μ), Eq. (81) is solved numerically to predict density profiles of single gas/liquid interfaces [109–111]. The spatially constant chemical potential, μ, is predetermined from the EOS at a set temperature [95,112]. Surface tension follows by quadrature [67,109–111].

Although written for a single-component, flat gas/liquid interface, Eq. (81) applies equally well to thin gas/liquid films with a simple change to a symmetry boundary condition at the film center. In a thin film, however, the chemical potential, μ, no longer characterizes saturated vapor/liquid phase equilibrium (i.e., μ^{sat}) because the film-meniscus liquid and the gas phase surrounding the film are not at the same pressure (i.e., there are 2 thermodynamic degrees of freedom). By definition from Eq. (2), this pressure difference gives the disjoining pressure. Upon fixing the bulk gas density, the chemical potential and the homogeneous gas pressure are calculated from the chosen EOS at the given temperature. Bulk liquid density in the meniscus is established from equality of chemical potential. Corresponding bulk liquid-meniscus pressure and, accordingly the disjoining pressure, follow from the EOS. Equivalently, the first equality in Eq. (45) [60] or Eq. (46) may be utilized to ascertain Π. Finally, the density profile is calculated from solution to Eq. (81) to assess the corresponding film-model thickness, h_1, according to Gibbs convention in Eq. (38). The calculation proceeds through different disjoining pressures and film thicknesses as different bulk gas densities are chosen. Additional detail is available in Appendix E.

In the case of a multicomponent mixture, gas density and composition are fixed at a given temperature. Equality of chemical potentials establishes the liquid density and composition. With densities and compositions set, gas and liquid pressures, and, hence, the disjoining pressure are calculated from the EOS. Again, the gas density is in the metastable phase plane and is not that corresponding to planar liquid/vapor equilibrium. Once the chemical potential of each component is known (from the set gas density and composition), the appropriate multicomponent embodiment of Eq. (81) [67,110] are solved to give density profiles and, finally, film thickness.

Because most equations of state account only for finite molecular size and attractive intermolecular interactions, thin-film forces from SGT are net attractive. Consequently, disjoining pressure is negative with liquid-meniscus pressure larger than that of the gas phase. Square-gradient theory thus predicts so-called Hamaker conjoining forces [63,64,73,113,114]. Calculation detail and chosen parameters for water are given in Appendix E using the Peng–Robinson EOS.

Fig. 19 gives predicted density profiles (compare Fig. 1) and tangential-stress profiles predicted from square-gradient theory for water at 479 K with $c = 4.95\times10^{-9}$ cm^8 bar/(mol)^2 and for two example values of film thickness: $h_1 = 1.3$ and 3.5 nm. The thicker film attains close to bulk liquid density and tangential stress (equal to the vapor pressure) at the film center. As portrayed in Figs. 21 and 22 below, the thick film exhibits a small negative disjoining pressure of about −0.001 MPa confirming weak attractive Hamaker forces. Conversely, the thinner of the two films does not attain bulk values at the film center and, by definition, is a thin film. It exhibits a significant attractive disjoining pressure of −14.5 MPa.

Fig. 20 quantifies the film thickness, h_m (defined in Eqs. (56) and (62)) as filled squares in the membrane model versus film

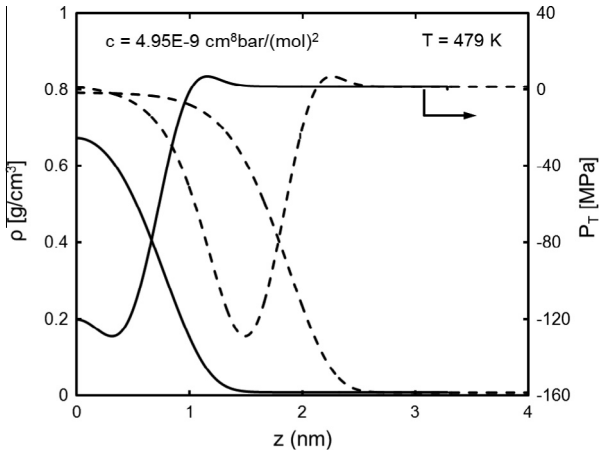

Fig. 19. Mass density and tangential stress profiles for water at 479 K from SGT and Peng–Robinson EOS. Dashes lines are for a thick film with $h_1 = 3.5$ nm evidenced by the near bulk density and stress at the film center. Solid lines correspond to a thin film with $h_1 = 1.3$ nm.

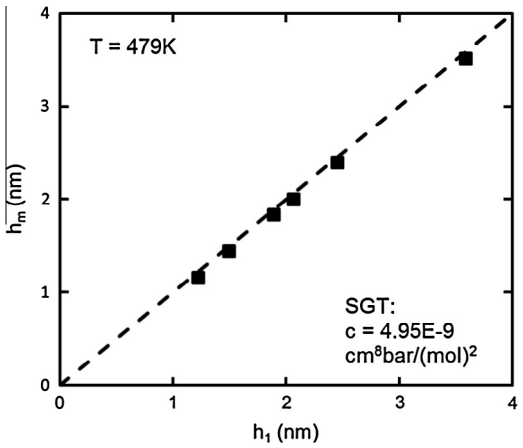

Fig. 20. Membrane-model thickness versus film-model thickness (filled squares) from SGT for water at 479 K and $c = 4.95 \times 10^{-9}$ cm^8 bar/(mol)^2. The dashed line indicates coincidence of the two thicknesses.

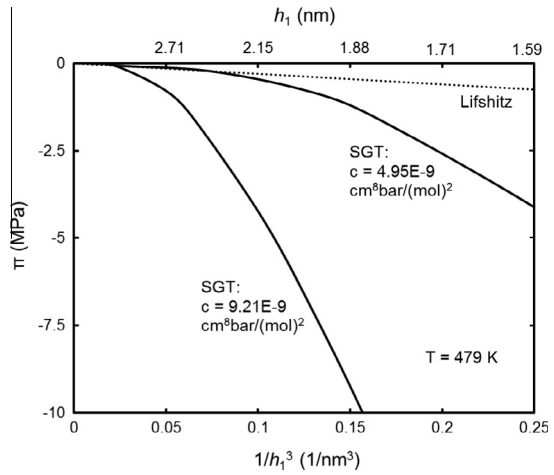

Fig. 21. Disjoining-pressure isotherms as a function of $1/h_1^3$ for water at 479 K from SGT and Peng–Robinson EOS. Solid lines correspond to two values of the influence parameter: $c = 4.95 \times 10^{-9}$ and 9.21×10^{-9} cm^8 bar/(mol)^2. The smaller value of c matches Lifshitz theory (dotted line) at large thickness, whereas the larger value of c matches the bulk surface tension.

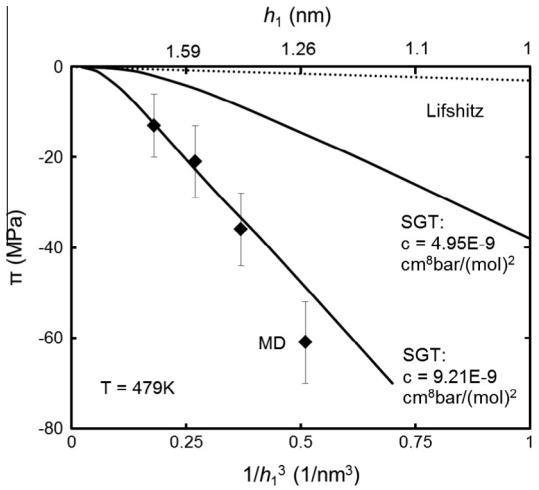

Fig. 22. Disjoining-pressure isotherms as a function of $1/h_1^3$ for water at 479 K from MD simulations (filled diamonds) [60] compared to SGT (solids lines). Lifshitz's theory is shown as a dotted line. Much larger attractive forces arise in thin films than predicted by Hamaker theory. Simulations are reprinted with permission from Bhatt et al. [60].

thickness, h_1 (defined in Eq. (38)) in the film model from SGT for water at 479 K. The dashed line designates exact agreement between the two thicknesses. Over the range of thickness probed, the difference between the two definitions is imperceptible.

Fig. 21 displays disjoining-pressure isotherms for water plotted as solid lines against $1/h_1^3$ suggested by Hamaker theory [63,64,73,113,114]. Also shown at the top of the figure are selected values of h_1. The straight dotted line corresponds to the Lifschitz's embodiment [60,114,115] of Hamaker theory for water taken from Bhatt et al. [60]. Two values of the influence parameter are illustrated: $c = 4.95 \times 10^{-9}$ and 9.21×10^{-9} cm^8 bar/(mol)^2. For all values of the influence parameter, SGT predicts that disjoining pressure approaches zero linearly in $1/h_1^3$ at large film thickness, consonant with Hamaker theory. The smaller value of the influence parameter in Fig. 21 is chosen so that disjoining pressure at large thickness coincides with the Lifshitz calculation. The larger value of c is chosen to reflect the experimental surface tension for water (35 mN/m). Disjoining pressures for this c value exhibit a Hamaker constant slightly smaller than that of Lifshitz (i.e., the linear slope at large film thickness in Fig. 21 is slightly smaller in magnitude than that of Lifshitz).

In all cases, however, SGT deviates significantly from Hamaker theory for thinner films. Although narrow portions of the SGT-predicted disjoining-pressure isotherms are linear in $1/h_1^3$, they are not so over a wide range. For thin films, disjoining pressures from SGT are much larger in magnitude compared to Hamaker theory. Although helpful for simple molecules, SGT is inappropriate for structured molecules as Eq. (81) cannot account for orientation changes near an interface. Our predictions for water disjoining pressures in Fig. 21 are illustrative.

4.2. Molecular simulation

Compared to wetting and confined films, molecular simulations of free thin liquid films are surprisingly rare. Most focus on the structure of NBFs [76,77,116–118] or film dynamics and rupture [74,119–121]. To our knowledge, only two groups have simulated disjoining-pressure isotherms for free thin liquid films. Bhatt et al. considered single-component SPC-E water [60] and Lennard-Jones (LJ) films [84]. Because only attractive forces are present with a positive-sloping disjoining-pressure isotherm, single-component

films are unstable. Nevertheless, the most probable mechanism of hydrodynamic curvature-driven film breakup commences at large disturbance wavelengths. Adequate simulation lateral box sizes are typically smaller than the critical wavelength for rupture (i.e., $\lambda_c \sim 2\pi\sqrt{\gamma/(d\Pi/dh)}$). Hence, purely attractive unstable films can be simulated. Very thin films, however, where $d\Pi/dh$ becomes large, cannot be maintained [74,119–121]. Moreover, simulations lose precision at larger film thicknesses. Only a limited range of thickness can, thus, be studied.

Fig. 22 shows as closed diamonds the molecular-dynamics (MD) disjoining-pressure simulations of SPC-E water films at 479 K from Bhatt et al. [60] again plotted against $1/h_1^3$. These points correspond to the mass-density profiles in Fig. 1. Similar to SGT, MD-simulated water films are considerably more attractive than those predicted by classical Hamaker theory (i.e., as estimated from Lifshitz's formulation [60,114,115]). Also shown for comparison are SGT predictions from Fig. 21. Disjoining pressures calculated with the larger value of c in Fig. 22 agree with those of MD from Bhatt et al. [60]. This comparison provides confidence in the results for both MD simulations and SGT. Presumably, MD simulation at large thicknesses conforms more closely to Hamaker theory than does SGT. Unfortunately, lack of precision in the MD simulations prevents consideration of thicker films where Hamaker theory applies. We conclude that the continuum approximation of a uniform-density liquid film in Hamaker's analysis is suspect for films thinner than about 8–10 molecular diameters.

Bhatt et al. [85] also simulated disjoining-pressure isotherms for surfactant-stabilized thin films, but with LJ surfactants in an LJ solvent. Repulsive disjoining pressures emerged originating from entropic overlap and interdigitation of the adsorbed nonionic-surfactant head groups [85]. More recently, Jang and Goddard [77] simulated aqueous surfactant-stabilized free thin films in the thickness range of Newton black films. Their disjoining-pressure isotherms are also repulsive and monotonically increasing for decreasing film thicknesses. The stated origin of the repulsive force is changes in solvation of counterions in NBFs compared to that in the bulk. Equilibration of film molecules with those in the surrounding bulk meniscus was apparently not attempted so no information is available on the role of surfactant (or indifferent-electrolyte) concentration on disjoining pressure.

5. Conclusions

Free liquid thin films display no bulk homogeneous densities. Rather, thin films exhibit inhomogeneous density profiles of component mass, stress, energy, entropy, etc. that do not attain bulk liquid values. Because of their thinness, thin-film forces arise, designated by Deryagin as disjoining (conjoining) pressures that are unique functions of film thickness. Disjoining pressure is a material property of the chemical system and, therefore, amenable to thermodynamic analysis.

The key to understanding thin-film thermodynamics is reversible mechanical work to expand/contract the film. When film expansion/contraction is carried out at constant thickness, a film model emerges in which the inhomogeneous film is replaced by a bulk liquid layer surrounded by a bulk gas phase. Excess film properties are attributed to two zero thickness membranes with film tension γ^f on each side of the film. Careful thermodynamic analysis of the film model leads to a thin-film Gibbs adsorption equation that relates film tension and disjoining pressure. A modified Young–Laplace equation is derived that reduces to the classical augmented Young–Laplace equation of Deryagin. Likewise, the classical Frumkin–Deryagin result is confirmed for the contact angle that the film makes with the bulk meniscus.

Conversely, when film expansion/contraction occurs at constant film volume, reversible mechanical work specifies a membrane model. In the membrane model, a single zero-thickness membrane appears with membrane tension, $2\gamma^m$, separating two bulk gas phases. There is no liquid film, only a single zero-volume membrane. A thin-film Gibbs adsorption equation in the membrane model relates membrane tension to disjoining pressure although with a different meaning for film thickness. No modified Young–Laplace equation applies in the membrane model. However, the film membrane does meet the bulk meniscus with a finite contact angle also given by the Frumkin–Deryagin formula. Comparison of the various mechanical work expressions provides a rigorous relation between film and membrane tensions.

Illustrative calculations of disjoining-pressure isotherms for water are presented by square-gradient theory (SGT) and molecular-dynamics (MD) simulations. SGT confirms Hamaker theory at large film thicknesses, but predicts considerably larger attractive forces for thin films of order 10 molecular diameters and less. MD confirms the SGT predictions at small film thicknesses and provides a more quantitative assessment.

Acknowledgments

Daniel Bregante performed the SGT calculations in Section 4.1. Tom Dursch provided helpful comments.

Appendix A. Film-model Gibbs invariants

When the locations of the dividing surfaces at $\pm h/2$ in the film model are altered, excess properties change. This situation is identical to that of changing the location of the Gibbs dividing surface for a single interface [78]. Let subscripts j and k denote locations of film half thickness, H_j and H_k, respectively. Then from Eq. (30), the excess film entropy per area of each dividing surface reads

$$s_k^f = s_j^f - \Delta\tilde{s}(H_k - H_j) \tag{A1}$$

Likewise film-model component adsorption of each dividing surface changes following Eq. (31)

$$\Gamma_{ik}^f = \Gamma_{ij}^f - \Delta\rho_i(H_k - H_j) \tag{A2}$$

Substitution of Eqs. (A1) and (A2) into Eq. (36) establishes that the coefficients multiplying dT and $d\mu_i$ are independent of a change in half thickness from H_j to H_k [78], whereas the coefficient multiplying dH is not.

Appendix B. Modified Young–Laplace equation

Volume and area expressions in Eq. (66) from Fig. 16 are given by: $V_L = 4w\int_0^L H(x)dx$, $V_G = 2w\tau L - V_L$, $A^{LG} = 2w\int_0^L \sqrt{1+H_x^2}dx$, $A^{SL} = 2wH_L$, and $A^{SG} = \tau w - A^{SL}$. Substitution of these expressions into Eq. (66) yields Eq. (67). Since the first and fourth terms on the right of Eq. (67) are constants, variational differentiation gives Eq. (68). It remains to evaluate the functional derivative of the integral in Eq. (68). Let $F(H, H_x; x)$ symbolize the integrand in Eq. (68). Euler–Lagrange conditions then read [122,123]

$$\delta\int_0^L \left[\gamma^f\sqrt{1+H_x^2} + P_c H\right]dx = \delta\int_0^L F(H,H_x;x)dx = \int_0^L \left[\frac{\partial F}{\partial H} - \frac{d}{dx}\left(\frac{\partial F}{\partial H_x}\right)\right]\delta H dx + \left(\frac{\partial F}{\partial H_x}\delta H\right)_0^L \tag{B1}$$

Evaluation of the derivatives in the last equality transforms this expression to

$$\delta\int_0^L\left[\gamma^f\sqrt{1+H_x^2}+P_CH\right]dx=\int_0^L\left[-\gamma^f\frac{H_{xx}}{(1+H_x^2)^{3/2}}+\frac{d\gamma^f}{dH}\frac{1}{(1+H_x^2)^{1/2}}+P_C\right]\delta H dx + \left(\gamma^f\frac{H_x}{(1+H_x^2)^{1/2}}\delta H\right)_0^L \tag{B2}$$

The second term on the right is zero at $x = 0$ because film half thickness is fixed at H_f. In this term at $x = L$, the solid/liquid contact angle is fixed and $\gamma^f = \gamma$. Geometry gives $H_x(L) = \mathrm{ctn}\theta$. Accordingly, the last term on the right reduces to

$$\left(\gamma^f\frac{H_x}{(1+H_x^2)^{1/2}}\delta H\right)_0^L=\gamma\cos\theta\delta H_L \tag{B3}$$

Substitution of Eqs. (B2) and (B3) into Eq. (68) of the text results in

$$0=\int_0^L\left[-\gamma^f\frac{H_{xx}}{(1+H_x^2)^{3/2}}+\frac{d\gamma^f}{dH}\frac{1}{(1+H_x^2)^{1/2}}+P_C\right]\delta H dx + (\gamma\cos\theta+\gamma^{SL}-\gamma^{SG})\delta H_L \tag{B4}$$

Because functional variations are arbitrary, each term on right of Eq. (B4) equals zero independently. This observation leads to Eqs. (69) and (70) of the text.

Appendix C. Film contact angle

Equality of x-forces per unit width of the rectangular parallelpiped in Fig. 17 reads

$$P_LH_f+P_G(H-H_f)+\gamma^f(H)\cos\varphi(H)=P_LH+\gamma^f(H_f) \tag{C1}$$

where H is the half thickness of the symmetric film. Substitution of Eq. (2) into Eq. (C1) gives Eq. (76) of the text. Resolution of z-forces is by symmetry.

Appendix D. Film contact angle from modified Young–Laplace

To derive an expression for the film contact angle from the modified Young–Laplace relation, Eq. (71) is rewritten as

$$\frac{d(yf)}{dh}+\frac{P_C}{2}=0 \tag{D1}$$

where $y(h)=1/\sqrt{1+H_x^2}=\cos\varphi$, $f(h)=\gamma+P_E(h)/2$, and the subscript unity on film thickness is dropped. Integration of Eq. (D1) yields

$$\cos\varphi=\frac{[1+P_E(h_f)/2\gamma]}{[1+P_E(h)/2\gamma]}-\frac{P_C(h-h_f)}{2\gamma[1+P_E(h)/2\gamma]} \tag{D2}$$

For large film thickness where disjoining forces disappear, Eq. (D2) reduces to

$$\cos\varphi=1+\frac{P_E(h_f)+P_Ch_f}{2\gamma}-\frac{P_Ch}{2\gamma} \tag{D3}$$

Thus, at large film thicknesses, cosine of the tangent angle is linear in film thickness. The intercept of that straight line gives the film contact angle [98,99]

$$\cos\theta_f=1+[P_Ch_f+P_E(h_f)]/2\gamma \tag{D4}$$

Substitution of Eqs. (2) and (15) into this expression gives Eq. (78) of the text.

Appendix E. Square-gradient theory for thin films (SGT)

Considerable detail is available on SGT using the Peng–Robinson EOS for single interfaces [109–111,124]. Here we provide a brief summary of the calculations appropriate to thin films. Before solving Eq. (81), the gas/liquid binodal phase boundary is located at the specified temperature. Simultaneous equality of chemical potentials (relative to a reference value)

$$\mu=\mu^*(T)-R_gT\ln\left(\frac{1-\rho b}{\rho b}\right)+\frac{\rho bR_gT}{1-\rho b}-\frac{\rho a}{1+2\rho b-(\rho b)^2} -\frac{a}{2\sqrt{2}b}\ln\left(\frac{1+\rho b(1+\sqrt{2})}{1+\rho b(1-\sqrt{2})}\right) \tag{E1}$$

and pressures

$$P=\frac{\rho R_gT}{1-\rho b}-\frac{\rho^2a}{1+2\rho b-(\rho b)^2} \tag{E2}$$

in the gas and liquid phases yields the saturated gas and liquid molar densities: ρ_G^{sat} and ρ_L^{sat} and, accordingly, the vapor pressure. In Eqs. (E1) and (E2), a and b are the Peng–Robinson interaction and size parameters, respectively. We chose $a = 7.2\times10^6$ cm^6 bar/(mol)^2 and $b = 17.204$ cm^3/mol.

These values give reasonable estimates for the saturated liquid density and vapor pressure for water at 479 K. Once ρ_G^{sat} and ρ_L^{sat} are known, the saturated bimodal chemical potential, μ^{sat}, is calculated from Eq. (E1).

To begin the thin-film density-profile calculation from Eq. (81), the bulk gas density is set in the spinodal region at a value above ρ_G^{sat}. Substitution of this value into Eq. (E1) specifies the constant chemical potential, μ, in Eq. (81). μ_o in this expression is a function of density following Eq. (E1). Solution to Eq. (81) is by a marching routine where Eq. (81) is re-written as two simultaneous first-order ordinary-differential equations. The algorithm marches the inhomogeneous density in position from the chosen gas-phase density toward that in the film center. Since the slope at the bulk gas density is zero, we employ an asymptotic expression to initiate the calculation

$$\rho(\bar{z})=\rho_G\left(1+\frac{\alpha}{c}\bar{z}^2\right) \tag{E3}$$

where

$$\alpha=\frac{R_gT}{\rho_G(1-\rho_Gb)}+\frac{a+bR_gT}{(1-\rho_Gb)^2}-\frac{a[1+(\rho_Gb)^2]}{[1+\rho_Gb-(\rho_Gb)^2]^2} \tag{E4}$$

and $\bar{z}$ is a linear coordinate of origin in the bulk gas phase and directed toward the film center. To start the marching process, a small enough value of $\bar{z}$ is chosen such that the final profile is independent of that choice. Marching continues until the maximum density at the film center is located. The $z = 0$ coordinate is then set at this position. Once the density profile is found, film thickness follows from the Gibbs construction in Eq. (38) with the liquid density set at ρ_L^{sat}. Disjoining pressure at this thickness follows from Eq. (46) as approximated by $\Pi=\rho_L^{sat}[\mu^{sat}-\mu(\rho_G)]$.

Thus, varying the gas density in the spinodal region allows construction of the disjoining-pressure isotherm. Tangential stress emerges from the density profile as [109–111,124]

$$P_T=P(\rho)-c\left[\rho\left(\frac{d^2\rho}{dz^2}\right)-\frac{1}{2}\left(\frac{d\rho}{dz}\right)^2\right] \tag{E5}$$

where local pressure, P, obeys Eq. (E2) at the local density. Surface tension for a bulk interface is given by quadrature from the expression [109–111,124]

$$\gamma=c\int_{-\infty}^{\infty}\left(\frac{d\rho}{dz}\right)^2dz \tag{E6}$$

References

[1] B.V. Deryagin, M.M. Kusakov, Izv. Akad. Nauk SSSR Ser. Khim. 5 (1936) 741 (in Russian).
[2] B.V. Deryagin, M.M. Kusakov, Izv. Akad. Nauk SSSR Ser. Khim. 6 (1937) 1119 (in Russian).
[3] B.V. Deryagin, Zh. Fis. Khim. 14 (1940) 137 (in Russian).
[4] B.V. Deryagin, Colloid J. USSR 17 (1955) 191.
[5] B.V. Deryagin, N.V. Churaev, J. Colloid Interface Sci. 66 (1978) 389.
[6] B.V. Deryagin, N.V. Churaev, V.M. Muller, Surface Forces, Consultants Bureau, Plenum Press, New York, 1987.
[7] A. Scheludko, Kolloid Zeit. 155 (1957) 39 (in German).
[8] A. Scheludko, Adv. Colloid Interface Sci. 1 (1967) 391.
[9] C. Stubenrauch, R. von Klitzing, J. Phys.: Condens. Matter 15 (2003) R1197.
[10] A.A. Rao, D.T. Wasan, E.D. Manev, Chem. Eng. Commun. 15 (1982) 63.
[11] E.D. Manev, S.V. Sazdanova, D.T. Wasan, J. Colloid Interface Sci. 97 (1984) 591.
[12] E.D. Manev, S.V. Sazdanova, D.T. Wasan, J. Dispersion Sci. Technol. 5 (1984) 111.
[13] A.K. Malhotra, D.T. Wasan, Chem. Eng. Commun. 48 (1986) 35.
[14] D.T. Wasan, A.K. Malhotra, AIChE Symp. Ser. Thin Film Phenom. 82 (1986) 5.
[15] A.K. Malhotra, D.T. Wasan, AIChE J. 33 (1987) 1533.
[16] A.D. Nikolov, D.T. Wasan, P.A. Kralchevsky, I.B. Ivanov, Ordered structures in thinning micellar foam and latex films, in: N. Ise, I. Sogami (Eds.), Yamada Conference Proceedings on Ordering and Organization in Ionic Solutions, Kyoto, Japan, World Scientific Co., Singapore, 1987, p. 302 (November).
[17] A.D. Nikolov, D.T. Wasan, J. Colloid Interface Sci. 133 (1989) 1.
[18] A.D. Nikolov, P.A. Kralchevsky, I.B. Ivanov, D.T. Wasan, J. Colloid Interface Sci. 133 (1989) 13.
[19] P.A. Kralchevsky, A.D. Nikolov, D.T. Wasan, I.B. Ivanov, Langmuir 6 (1990) 1180.
[20] A.D. Nikolov, D.T. Wasan, N.D. Denkov, P.A. Kralchevsky, I.B. Ivanov, Prog. Colloid Polym. Sci. 87 (1990) 87.
[21] E.S. Basheva, A.D. Nikolov, P.A. Kralchevsky, I.B. Ivanov, D.T. Wasan, Multi-stepwise drainage and viscosity of macroscopic films formed from latex suspensions, in: K.L. Mittal, D.O. Shah (Eds.), Surfactants in Solution, vol. II, Plenum Press, New York, 1991, p. 467.
[22] D.T. Wasan, A.D. Nikolov, P.A. Kralchevsky, I.B. Ivanov, Colloids Surf. 67 (1992) 139.
[23] A.D. Nikolov, D.T. Wasan, Langmuir 8 (1992) 2985.
[24] D.T. Wasan, A.D. Nikolov, P.A. Kralchevsky, I.B. Ivanov, Foam film stability: Role of micellar interactions on the formation and expansion of spots in stratifying film. An overview, in: M.G. Velarde, C.I. Christov (Eds.), Fluid Physics, Lecture Notes of Summer Schools. World Scientific Series on Nonlinear Science, Series B, vol. 5, 1994, p. 209.
[25] X.L. Chu, A.D. Nikolov, D.T. Wasan, J. Chem. Phys. 103 (1995) 6653.
[26] K. Koczo, A.D. Nikolov, D.T. Wasan, R.P. Borwankar, A. Gonsalves, J. Colloid Interface Sci. 178 (1996) 694.
[27] A.D. Nikolov, D.T. Wasan, S.E. Friberg, Colloids Surf. 118 (1996) 221.
[28] Y.H. Kim, D.T. Wasan, J. Ind. Eng. Chem. (Seoul) 3 (1997) 128.
[29] A.D. Nikolov, D.T. Wasan, Colloids Surf. 128 (1997) 243.
[30] D.T. Wasan, A.D. Nikolov, X.L. Chu, An overview of depletion and surface-induced structural forces in thin micellar films, in: D.O. Shah (Ed.), Micelles, Microemulsions, and Monolayers, Science and Technology, Marcel Dekker, Inc., New York, 1998, p. 124.
[31] D.T. Wasan, A. Nikolov, A. Trokhymchuk, D. Henderson, Condens. Matter Phys. 4 (2001) 361.
[32] G. Sethumadhavan, S. Bindal, A. Nikolov, D.T. Wasan, Colloids Surf. 204 (2002) 51.
[33] K. Kumar, A.D. Nikolov, D.T. Wasan, J. Colloid Interface Sci. 256 (2002) 194.
[34] A. Trokhymchuk, D. Henderson, A.D. Nikolov, D.T. Wasan, J. Phys. Chem. B 107 (2003) 3927.
[35] G. Sethumadhavan, A. Nikolov, D. Wasan, J. Colloid Interface Sci. 272 (2004) 167.
[36] A.D. Nikolov, D.T. Wasan, Micellar films: thinning and structure, in: P. Somasundaran (Ed.), Encyclopedia of Surface and Colloid Science, second ed., Marcel Dekker, New York, 2006.
[37] A.D. Nikolov, D.T. Wasan, Nonionic micelle films: thinning and stability, in: T. Tadros (Ed.), Colloid Stability – The Role of Surface Forces, Colloid and Interface Science Series, vol. 3, Wiley-VCH, Weinheim, 2007, p. 397.
[38] G.A. Martynov, B.V. Deryagin, Colloid J. USSR 24 (1962) 411.
[39] B.V. Deryagin, G.A. Martynov, Y.V. Gutop, Colloid J. USSR 27 (1965) 298.
[40] A.I. Rusanov, Colloid J. USSR 28 (1966) 583.
[41] A.I. Rusanov, Colloid J. USSR 29 (1967) 118.
[42] A.I. Rusanov, Colloid J. USSR 29 (1967) 183.
[43] A.I. Rusanov, Thermodynamics of films, in: B.V. Deryagin (Ed.), Research in Surface Forces, vol. 3, Consultants Bureau, Plenum Press, New York, 1971, p. 103.
[44] A.I. Rusanov, J. Colloid Interface Sci. 53 (1975) 20.
[45] B.V. Toshev, I.B. Ivanov, Colloid Polym. Sci. 253 (1975) 558.
[46] I.B. Ivanov, B.V. Toshev, Colloid Polym. Sci. 253 (1975) 593.
[47] J.A. De Feijter, J.B. Rijnbout, A. Vrij, J. Colloid Interface Sci. 64 (1978) 258.
[48] B.V. Toshev, Colloids Surf. 2 (1981) 243.
[49] J.C. Erikson, B.V. Toshev, Colloids Surf. 5 (1982) 241.
[50] A. Marmur, J. Colloid Interface Sci. 93 (1983) 18.
[51] J.A. de Feijter, Thermodynamics of thin liquid films, in: I.B. Ivanov (Ed.), Thin Liquid Films: Fundamentals and Applications, vol. 29, Marcel Dekker, New York, 1988, p. 1.
[52] G.J. Hirasaki, Thermodynamics of thin films and three-phase contact regions, in: N.R. Morrow (Ed.), Interfacial Phenomena in Petroleum Recovery, vol. 36, Marcel Dekker, New York, 1990, p. 23 (Chapter 2).
[53] D. Li, A.W. Neumann, Adv. Colloid Interface Sci. 36 (1991) 125.
[54] V.G. Babak, Russ. Chem. Rev. 62 (1993) 11.
[55] A. Amirfazli, J. Adhes. 80 (2004) 1003.
[56] A.I. Rusanov, Surf. Sci. Rep. 58 (2005) 11.
[57] V.M. Starov, M.G. Velarde, C.J. Radke, Dynamics of Wetting and Spreading, Surfactant Science Series, vol. 138, Taylor & Frances, Boca Raton, 2007.
[58] A.I. Rusanov, Colloid J. 69 (2007) 39.
[59] A.N. Frumkin, Zh. Fiz. Khim. 12 (1938) 337 (in German).
[60] D. Bhatt, J. Newman, C.J. Radke, J. Phys. Chem. B 107 (2003) 13076.
[61] K.J. Mysels, K. Shinoda, S. Frankel, Soap Films: Studies of their Thinning, Pergamon Press, New York, 1959.
[62] A.W. Adamson, A.P. Gast, Physical Chemistry of Surfaces, sixth ed., John Wiley & Sons Inc., New York, 1977.
[63] J.C. Berg, An Introduction to Interfaces & Colloids: The Bridge to Nanoscience, World Scientific, New Jersey, 2010.
[64] R. Defay, I. Prigogine, A. Bellmans, D.H. Everett, Surface Tension and Adsorption, John Wiley & Sons Inc., New York, NY, 1966.
[65] J.S. Rowlinson, B. Widom, Molecular Theory of Capillarity, Dover Publications Inc., Mineola, New York, 1982.
[66] I.B. Ivanov, P.A. Kralchevsky, Mechanics and thermodynamics of curved thin films, in: I.B. Ivanov (Ed.), Thin Liquid Films: Fundamentals and Applications, vol. 29, Marcel Dekker, New York, 1988, p. 49 (Chapter 2).
[67] H.T. Davis, Statistical Mechanics of Phases, Interfaces, and Thin Films, VCH Publishers Inc., New York, 1996.
[68] K.J. Mysels, M.N. Jones, Discuss. Faraday Soc. 42 (1966) 42.
[69] V. Bergeron, C.J. Radke, Langmuir 8 (1992) 3020.
[70] V. Bergeron, J. Phys.: Condens. Matter 11 (1999) R215.
[71] A.S. Aronson, V. Bergeron, M.E. Fagan, C.J. Radke, Colloids Surf. A: Physicochem. Eng. Aspects 83 (1994) 109.
[72] V. Bergeron, A.I. Jimenez-Laguna, C.J. Radke, Langmuir 8 (1992) 3027.
[73] J.Th.G. Overbeek, The interaction between colloidal particles, in: H.R. Kruyt (Ed.), Colloid Science I Irreversible Systems, Elsevier, Amsterdam, 1952.
[74] W. Yang, R. Wu, B. Kong, X. Zhang, X. Yang, J. Phys. Chem. B 113 (2009) 8332.
[75] O. Bélorgey, J. Benattar, Phys. Rev. Lett. 66 (1991) 313.
[76] Z. Gamba, J.J. Hautman, J.C. Shelley, M.L. Klein, Langmuir 8 (1992) 3155.
[77] S.S. Jang, W.A. Goddard III, J. Phys. Chem. B 110 (2006) 7992.
[78] C.J. Radke, Adv. Colloid Interface Sci. doi: http://dx.doi.org/10.1016/j.cis.2014.01.001.
[79] S.G. Ash, D.H. Everett, C.J. Radke, J. Chem. Soc. – Faraday Trans. II 69 (1973) 1256.
[80] D.G. Hall, J. Chem. Soc. – Faraday Trans. II 68 (1972) 2169.
[81] I. Prigogine, R. Defay, Chemical Thermodynamics (D.H. Everett, Trans.), Longman, London, 1954.
[82] E.A. Guggenheim, Thermodynamics, fifth ed., North-Holland, Amsterdam, 1967.
[83] J.W. Gibbs, Collected Works, vol. 1, Yale University Press, New Haven, CN, 1961. pp. 219–314.
[84] D. Bhatt, J.S. Newman, C.J. Radke, J. Phys. Chem. B 106 (2002) 6529.
[85] D. Bhatt, J.S. Newman, C.J. Radke, J. Phys. Chem. B 18 (2004) 13412.
[86] D.H. Napper, Polymeric Stabilization of Colloidal Dispersions, Academic Press, New York, 1983 (Chapter 10).
[87] V. Subramanian, W. Ducker, J. Phys. Chem. B 105 (2001) 1389.
[88] W.J. Lokar, W.A. Ducker, Langmuir 18 (2002) 3167.
[89] W.J. Lokar, L.K. Koopal, F.-A.M. Leermakers, W.A. Ducker, J. Phys. Chem. B 108 (2004) 3633.
[90] W.J. Lokar, W.A. Ducker, Langmuir 20 (2004) 4553.
[91] W.J. Lokar, L.K. Koopal, F.-A.M. Leermakers, W.A. Ducker, J. Phys. Chem. B 108 (2004) 15033.
[92] L.K. Koopal, F.-A.M. Leermakers, W.J. Lokar, W.A. Ducker, Langmuir 21 (2005) 10089.
[93] F.-A.M. Leermakers, L.K. Koopal, W.J. Lokar, W.A. Ducker, Langmuir 21 (2005) 11534.
[94] W.J. Lokar, W.A. Ducker, Colloids Surf. A 322 (2008) 256.
[95] J.M. Prausnitz, R.N. Lichtenthaler, E.G. de Azevedo, Molecular Thermodynamics of Fluid Phase Equilibria, third ed., Prentice Hall, New Jersey, 1999.
[96] P.G. de Gennes, F. Brocahrd-Wyart, D. Quéré, Capillarity and Wetting Phenomena: Drops, Bubbles, Pearls, Waves, Springer, USA, 2004.
[97] E.H. Yeh, J.S. Newman, C.J. Radke, Colloids Surf. A 156 (1999) 137.
[98] E.H. Yeh, J.S. Newman, C.J. Radke, Colloids Surf. A 156 (1999) 525.
[99] T. Yi, H. Wong, J. Colloid Interface Sci. 313 (2007) 579.
[100] B. Dai, L.G. Leal, Phys. Rev. E 78 (2008) 061602.
[101] D. Silin, G. Virnovsky, Transport Porous Media 82 (2010) 485.
[102] V.M. Starov, Wetting, in: T. Tadros (Ed.), Encyclopedia of Colloid and Interface Science, Springer-Verlag, Berlin, 2013, p. 1399.
[103] I.V. Kuchin, O.K. Matar, R.V. Craster, V.M. Starov, Soft Matter 10 (2014) 6024.
[104] G. Hirasaki, SPE Form. Eval. (1991) 217
[105] J.A. De Feijter, A. Vrij, J. Electroanal. Chem. 37 (1972) 9.
[106] V.M. Starov, Adv. Colloid Interface Sci. 161 (2010) 139.

[107] G. Rickayzen, P. Richmond, Statistical mechanics of inhomogeneous films of nonelectrolytes, in: I.B. Ivanov (Ed.), Thin Liquid Films: Fundamentals and Applications, vol. 29, Marcel Dekker, New York, 1988, p. 131 (3).
[108] J.W. Cahn, J.E. Hilliard, J. Chem. Phys. 28 (1958) 258.
[109] B.S. Carey, L.E. Scriven, H.T. Davis, AIChE J. 24 (1978) 1076.
[110] B.S. Carey, L.E. Scriven, H.T. Davis, AIChE J. 26 (1980) 705.
[111] J.M. Nitsche, G.F. Teletzke, L.E. Scriven, H.T. Davis, Fluid Phase Equilb. 14 (1983) 203.
[112] A. Firoozabadi, Thermodynamics of Hydrocarbon Reservoirs, McGraw-Hill, New York, 1999.
[113] H.C. Hamaker, Physica 4 (1937) 1058.
[114] J.N. Israelachvili, Intermolecular and Surface Forces, second ed., Academic Press, Waltham, MA, 1991 (Chapter 11).
[115] R.R. Dagastine, D.C. Prieve, L.R. White, J. Colloid Interface Sci. 231 (2000) 351.
[116] F. Bresme, J. Faraudo, Langmuir 20 (2004) 5127.
[117] J. Faraudo, F. Bresme, Phys. Rev. Lett. 92 (2004) 236102.
[118] J. Faraudo, F. Bresme, Phys. Rev. Lett. 94 (2005) 077802.
[119] C.-C. Hwang, J.-Y. Hsieh, K.-H. Chang, J.-J. Liao, Physica A 256 (1998) 333.
[120] J.G. Weng, S. Park, J.R. Lukes, C.-L. Tien, J. Chem. Phys. 113 (2000) 5917.
[121] T. Kuznicki, J.H. Masliyah, S. Bhattacharjee, Langmuir 23 (2007) 1782.
[122] V.S. Arpaci, Conduction Heat Transfer, Addison-Wesley, Reading, MA, 1966 (Chapter 8).
[123] F.B. Hildebrand, Advanced Calculus for Applications, second ed., Prentice-Hall, Englewood Cliffs, New Jersey, 1976 (Chapter 7).
[124] G.F. Teletzke, L.E. Scriven, H.T. Davis, J. Colloid Interface Sci. 87 (1982) 550.